J. Fluid Mech. (2010), *vol.* 664, *pp.* 348–396. © Cambridge University Press 2010
doi:10.1017/S0022112010003794

Modelling dynamic and irreversible powder compaction

RICHARD SAUREL[1,2]†, N. FAVRIE[1], F. PETITPAS[1], M.-H. LALLEMAND[1] AND S. L. GAVRILYUK[1]

[1]SMASH Project-team, UMR CNRS 6595 IUSTI – INRIA, Polytech Marseille, Aix-Marseille Université, 5 rue E. Fermi, 13 453 Marseille CEDEX 13, France

[2]University Institute of France, Polytech Marseille, Aix-Marseille Université, 5 rue E. Fermi, 13 453 Marseille CEDEX 13, France

(Received 12 March 2009; revised 9 July 2010; accepted 12 July 2010; first published online 1 November 2010)

A multiphase hyperbolic model for dynamic and irreversible powder compaction is built. Four important points have to be addressed in this case. The first one is related to the irreversible character of powder compaction. When a granular media is subjected to a loading–unloading cycle, the final volume is lower than the initial one. To deal with this hysteresis phenomenon, a multiphase model with relaxation is built. During loading, mechanical equilibrium is assumed corresponding to stiff mechanical relaxation, while during unloading non-equilibrium mechanical transformation is assumed. Consequently, the sound speed of the limit models are very different during loading and unloading. These differences in acoustic properties are responsible for irreversibility in the compaction process. The second point is related to dynamic effects, where pressure and shock waves play an important role. Wave dynamics is guaranteed by the hyperbolic character of the equations. Phase compressibility as well as configuration energy are taken into account. The third point is related to multi-dimensional situations that involve material interfaces. Indeed, most processes with powder compaction entail *free surfaces*. Consequently, the model should be able to solve interfaces separating pure fluids and granular mixtures. Finally, the fourth point is related to gas permeation that may play an important role in some specific powder compaction situations. This poses the difficult question of multiple-velocity description. These four points are considered in a unique model fitting the frame of multiphase theory of diffuse interfaces (Saurel & Abgrall, *J. Comput. Phys.*, vol. 150, 1999, p. 425; Kapila *et al.*, *Phys. Fluids*, vol. 13, 2001, p. 3002; Saurel *et al.*, *J. Comput. Phys.*, vol. 228, 2009, p. 1678). The ability of the model to deal with these various effects is validated on basic situations, where each phenomenon is considered separately. Except for the material EOS (hydrodynamic and granular pressures and energies), which are determined on the basis of separate experiments found in the literature, the model is free of adjustable parameter.

Key words: granular media, particle/fluid flows, shock waves

† Email address for correspondence: richard.saurel@polytech.univ-mrs.fr

https://doi.org/10.1017/S0022112010003794 Published online by Cambridge University Press

1. Introduction

When a granular bed is subjected to mechanical loading, local deformations occur resulting in rearranged deformed grains that form a compact porous solid. Such a process is irreversible. As a matter of fact, if the loading stress is removed, the porous solid slightly expands but never turns back to its initial volume. The main difficulty in modelling such an effect relies on its irreversible character.

The literature on powder compaction provides at least three types of models.

(i) The first one is connected to the quasi-static plasticity modelling in solids (Gethin *et al.* 1994; Alderborn & Nyström 1996; Oliver, Oller & Cante 1996; Lewis & Khoei 2001). This approach usually considers powder mixture compressibility but neglects the solid-phase one. This restricts these models to weak compression waves, excluding strong shocks.

(ii) The second one considers granular media at the discrete level, where a large number of particles are simulated by considering contact forces between them (Martin, Bouvard & Shima 2003).

(iii) The third one deals with multiphase flow modelling of granular media (Baer & Nunziato 1986; Bdzil *et al.* 1999; Saurel & Abgrall 1999; Kapila *et al.* 2001; Chinnayya, Daniel & Saurel 2004; Murrone & Guillard 2005).

In this work, irreversible compaction of powders is addressed in the context of multiphase flow theory of granular materials. There are some advantages with this approach. First, large-scale experiments and engineering applications are easier to address with a continuous model of heterogeneous media. Second, wave dynamics is of fundamental importance in many applications dealing with shocks and explosions. Some success has been reached in this area with Baer & Nunziato (1986) type models, except for the two following issues.

First, this type of model cannot predict compacted powder zones after loading–unloading cycles that may occur, for example, after compression and expansion of a given granular sample. Progress in this direction was done by Gonthier (2003, 2004).

Second, the original formulation cannot solve interface problems, or material interfaces such as those separating a fluid and a granular mixture. Methods to solve interface conditions in the context of compressible fluids governed by different equations of state (EOS) have been built during the last two decades with the pioneer works of Karni (1994) and Abgrall (1996). Multiphase flow models have been used in this aim (Saurel & Abgrall 1999) in order to solve interface conditions with correct thermodynamics at interfaces, but in the context of fluid–fluid interfaces only.

The goal of this paper is to build a multiphase flow model, which is able to deal with irreversible compaction and to solve interfaces separating fluids and granular mixtures, in the presence of pressure waves.

To do so, we first build a mechanical equilibrium model, with a single velocity and a single stress. For that purpose, we assume that the energy of the system is the sum of the hydrodynamic energy plus a *configuration* (or *granular*) energy that depends on other variables, such as volume fractions, particle radius, specific volumes and entropies. The concept of *configuration pressure*, or *granular pressure*, is introduced, in particular, in Passman, Nunziato & Walsh (1984). We then expect the flow model to respect conservation of mass, mixture momentum and mixture energy and also to be adiabatic. From these constraints, the pressure definition that appears in the momentum equation is obtained, as well as the mechanical equilibrium condition. This analysis is carried out in § 2. However, this mechanical equilibrium model, already presented by Kapila *et al.* (2001), is reversible. It is

https://doi.org/10.1017/S0022112010003794 Published online by Cambridge University Press

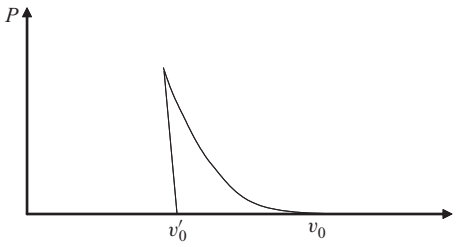


FIGURE 1. Schematic representation of a loading–unloading cycle for a powder sample, in the plane P–v.

therefore unable to predict the hysteresis phenomenon, such as compaction. In order to model irreversibility the following phenomenon is observed: consider a loading–unloading cycle as shown in figure 1 in the plane $P-v$ (P: stress, v: mixture specific volume). During the compression stage, the mixture-specific volume decreases and reaches its minimum value for the applied stress. During unloading, the pressure variation is stiff for a small specific volume variation. It means that the mixture sound speed,

$$c^2 = -v^2 \frac{\partial P}{\partial v}\Big)_s, \tag{1.1}$$

in the compression stage is much lower than the one involved in the expansion stage. Based on this observation, we are going to build a non-equilibrium model that possesses two limit sound speeds:

(i) An *equilibrium* sound speed corresponding to those of the mechanical equilibrium models. This sound speed will be the lowest one and will show up during the compression stage.

(ii) A *frozen* sound speed, which will be larger than the preceding one that will show up during the expansion stage.

The general model will be thus a non-equilibrium model with relaxation. The relaxation term expresses the degree of local stress disequilibrium. When the relaxation time tends to infinity, the frozen sound speed is recovered and used during the expansion stage, while when the relaxation time tends to zero, the asymptotic limit of the non-equilibrium model corresponds to the mechanical equilibrium model. This model, with low sound speed, will be used during compression. Then the non-equilibrium model couples two limit models: with frozen sound speed on the one hand and equilibrium sound speed on the other hand, by using a unique formulation. The switch from one limit model to the other one is achieved by means of the relaxation parameter. Before examining the details of this relaxation *switch*, the non-equilibrium model with relaxation is studied in § 3. Thermodynamic closure of both models is addressed in § 4, where thermodynamic EOS are presented, in addition to a new granular EOS. To solve the flow model, a numerical method is needed. The system consists of a non-conservative hyperbolic set of equations with relaxation. A similar system has been studied in the context of fluid mixtures by Saurel, Petitpas & Berry (2009). Extension of this method to the granular flow model is detailed in § 5. Validations are then addressed in § 6. The ability of the model to propagate compression and expansion waves, as well as its capabilities

https://doi.org/10.1017/S0022112010003794 Published online by Cambridge University Press

to capture fluid–granular mixtures interfaces, is demonstrated. Comparisons with several experiments are done, in particular, regarding the successive hysteresis-type loading–unloading cycles. In § 7, discussion about the relaxation parameter switch is given on the basis of basic plasticity theory arguments, combined with an analysis of the various non-equilibrium stages that occur during the compaction process. This discussion intends to justify the switch. We show, in particular, that the model is free of parameters. In § 8, the flow model is extended to gas permeation effects. A Darcy-type law, obtained from the asymptotic analysis of the Baer & Nunziato (1986) model in the limit of stiff mechanical relaxation is obtained, following Guillard & Duval (2007). Corresponding drift effects are thus restored in the Kapila *et al.* (2001) mechanical equilibrium model in a thermodynamically consistent manner, based on entropy production analysis (Saurel, Petitpas & Abgrall 2008). The corresponding velocity non-equilibrium model is validated against shock tube experiments, involving shock interaction with dense granular beds, showing excellent agreement in § 9. Conclusions are given in § 10.

2. Mechanical equilibrium model

A granular medium is different from a fluid mixture by several aspects, one of them being the presence of inter-granular contacts. Due to grain contacts the medium presents resistance to compression related to efforts that exert in the grains around each contact point. At the macroscopic scale, these efforts can be summarized with an additional EOS that expresses the compression resistance, with the help of a *granular pressure* or *configuration pressure*. The configuration energy associated to that configuration pressure can be derived. It can be understood as the energy stored in elastic–plastic layers around each contact point.

Granular pressure as a function of solid volume fraction can be determined easily by experimental means. An excellent description of experimental facility and corresponding measurements are given in Kuo, Yang & Moore (1980).

There are some advantages with this thermodynamic approach based on *configuration* pressure and energy. The effects occurring at grain scale, such as rearrangements and plastic deformations, are summarized in simple functions linking macroscopic variables. Therefore, the difficulty of solving complex multi-dimensional effects at grain scale is replaced by the experimental determination of *granular* EOS parameters.

The aim of this section is to develop a flow model involving these physical effects specific to granular media. The model building method consists in taking the total system energy as a function of the various problem variables and obtains:

(i) the mechanical equilibrium condition,

(ii) the form of the pressure term that exerts in the momentum equation.

The mechanical equilibrium condition is then differentiated along a particle trajectory, and therefore provides the volume fraction evolution equation that closes the system of classical balance equations: mass conservation for each phase, momentum and energy conservation for the mixture, entropy conservation for each phase and conservation of the number of particles per unit volume.

Let us assume that the total energy of the system is the sum of the classical thermodynamic internal energy augmented by the configuration (or granular) energy B plus the kinetic energy:

$$E = e + B + \tfrac{1}{2}u^2, \tag{2.1}$$

https://doi.org/10.1017/S0022112010003794 Published online by Cambridge University Press

with $e = \sum_k Y_k\, e_k(v_k, s_k)$ and $B = \sum_k Y_k\, B_k(\alpha_k, R_k, v_k, s_k, Y_k)$. Here $k = 1, 2$. For example, $k = 1$ corresponds to the solid phase and $k = 2$ corresponds to the gas phase. In that case, $B_2 = 0$. However, we keep that general formulation as it is more convenient to get symmetrized relations in what follows.

With this definition, the internal energy e_k of each phase depends on two thermodynamic variables: the specific volume v_k and the specific entropy s_k. The configuration energy B_k, associated with the solid deformed layers around each grain surface, is assumed to be a function of four variables, $B_k = B_k(\alpha_k, R_k, v_k, s_k, Y_k)$, where:

(i) α_k is the volume fraction of phase k, the dependence of which is obvious, since it is well known that the energy to transfer into a granular bed is a function of the volume fraction at the end of the compaction process;

(ii) R_k is the particle radius of the grains. Dependence on that variable cannot be excluded *a priori*;

(iii) the thermodynamic variables (v_k, s_k) may also influence the value of B_k;

(iv) $Y_k = (\alpha_k \rho_k)/\rho$ is the mass fraction, $\rho_k = 1/v_k$ is the density and $\rho = \sum_k (\alpha_k \rho_k)$ is the mixture density.

It is more convenient for the calculations to express the mixture total energy as a function of the following variables:

$$E = \sum_k Y_k\, [e_k(v_k, s_k) + B_k(\alpha_k, n_k, v_k, s_k, Y_k)] + \frac{1}{2} u^2, \tag{2.2}$$

where n_k represents the number of particles per unit mass. The particle radius R_k, considered spherical, is linked to the preceding variables by

$$v_k\, Y_k = \tfrac{4}{3}\, \pi\, R_k^3\, n_k. \tag{2.3}$$

Let us define

$$\frac{\mathrm{d}}{\mathrm{d}t} = \frac{\partial}{\partial t} + u\, \frac{\partial}{\partial x}, \tag{2.4}$$

then the classical balance laws are given below:

$$\frac{\partial \rho}{\partial t} + \frac{\partial (\rho u)}{\partial x} = 0, \quad \text{mixture mass conservation,} \tag{2.5}$$

$$\frac{\mathrm{d} Y_k}{\mathrm{d}t} = 0, \quad \text{mass conservation for phase } k, \tag{2.6}$$

$$\frac{\mathrm{d} s_k}{\mathrm{d}t} = 0, \quad \text{entropy conservation for phase } k, \tag{2.7}$$

$$\frac{\partial (\rho u)}{\partial t} + \frac{\partial \left(\rho u^2 + P\right)}{\partial x} = 0, \quad \text{mixture momentum conservation,} \tag{2.8}$$

$$\frac{\partial (\rho E)}{\partial t} + \frac{\partial ((\rho E + P)\, u)}{\partial x} = 0, \quad \text{total mixture energy conservation.} \tag{2.9}$$

In the absence of particle coalescence or breakup, the number of particles per unit volume reads as

$$\frac{\partial N_k}{\partial t} + \frac{\partial (N_k\, u)}{\partial x} = 0. \tag{2.10}$$

It can also be expressed as

$$\frac{\mathrm{d} n_k}{\mathrm{d}t} = 0 \quad \text{with } n_k = \frac{N_k}{\rho}. \tag{2.11}$$

https://doi.org/10.1017/S0022112010003794 Published online by Cambridge University Press

In (2.8) the pressure P is an unknown function that needs to be determined. Note that the phase entropies are assumed to be constant along their trajectories, meaning the transformations (loading and unloading) are reversible with this model. The irreversible character of compaction process will be addressed later with the non-equilibrium model.

By combining momentum and energy equations, the mixture internal energy equation is readily obtained:

$$\frac{\mathrm{d}(e+B)}{\mathrm{d}t} + P\frac{\mathrm{d}v}{\mathrm{d}t} = 0 \tag{2.12}$$

with

$$e + B = \sum_k Y_k \left[e_k(v_k, s_k) + B_k(\alpha_k, n_k, v_k, s_k, Y_k)\right]. \tag{2.13}$$

Using (2.5)–(2.11), the derivative of the mixture internal energy (2.12) along a trajectory becomes

$$\frac{\mathrm{d}(e+B)}{\mathrm{d}t} = \sum_k Y_k \left[\frac{\partial e_k}{\partial v_k}\right)_{s_k} \frac{\mathrm{d}v_k}{\mathrm{d}t} + \frac{\partial B_k}{\partial \alpha_k}\Big)_{n_k, v_k, s_k, Y_k} \frac{\mathrm{d}\alpha_k}{\mathrm{d}t} + \frac{\partial B_k}{\partial v_k}\Big)_{n_k, \alpha_k, s_k, Y_k} \frac{\mathrm{d}v_k}{\mathrm{d}t}\Bigg]. \tag{2.14}$$

But

$$P_k = -\frac{\partial e_k}{\partial v_k}\Big)_{s_k} \quad \text{and} \quad v_k = \frac{\alpha_k}{Y_k}\, v, \tag{2.15}$$

thus

$$\mathrm{d}v_k = \frac{\alpha_k}{Y_k}\,\mathrm{d}v + \frac{v}{Y_k}\,\mathrm{d}\alpha_k. \tag{2.16}$$

Consequently, (2.14) becomes

$$\begin{aligned}\frac{\mathrm{d}(e+B)}{\mathrm{d}t} + \frac{\mathrm{d}v}{\mathrm{d}t} \sum_k \alpha_k \left[P_k - \frac{\partial B_k}{\partial v_k}\Big)_{\alpha_k, n_k, s_k, Y_k}\right] \\ = v\left[\sum_k \left\{\frac{\partial B_k}{\partial v_k}\Big)_{\alpha_k, n_k, s_k, Y_k} - P_k + \alpha_k \rho_k \frac{\partial B_k}{\partial \alpha_k}\Big)_{n_k, v_k, s_k, Y_k}\right\} \frac{\mathrm{d}\alpha_k}{\mathrm{d}t}\right].\end{aligned} \tag{2.17}$$

This result has to be in concordance with (2.12), that is a consequence of energy, momentum and mass conservation. In order that (2.17) and (2.12) are in agreement, it is sufficient to set

$$P = \sum_k \alpha_k \left(P_k - \frac{\partial B_k}{\partial v_k}\Big)_{\alpha_k, n_k, s_k, Y_k}\right), \tag{2.18}$$

and, for all k, j, $k \neq j$:

$$\frac{\partial B_k}{\partial v_k}\Big)_{\alpha_k, n_k, s_k, Y_k} - P_k + \alpha_k \rho_k \frac{\partial B_k}{\partial \alpha_k}\Big)_{n_k, v_k, s_k, Y_k} = \frac{\partial B_j}{\partial v_j}\Big)_{\alpha_j, n_j, s_j, Y_j} - P_j + \alpha_j \rho_j \frac{\partial B_j}{\partial \alpha_j}\Big)_{n_j, v_j, s_j, Y_j}. \tag{2.19}$$

Equation (2.18) corresponds to the mixture pressure definition. Equation (2.19) represents the mechanical equilibrium condition. These two definitions are consequences of the choice of the system energy subjected to the constraints (2.5)–(2.11).

https://doi.org/10.1017/S0022112010003794 Published online by Cambridge University Press

Dependence on phase compressibility is usually neglected during the compaction process. Indeed, at moderate loading, particles deform but nearly conserve their volume. When loading increases, bed porosity decreases and compressible effects become gradually important, typically for pressures greater than 100 MPa. Thus, it is commonly assumed that

$$\frac{\partial B_k}{\partial v_k}\Big)_{\alpha_k,n_k,s_k,Y_k} = 0. \tag{2.20}$$

The mechanical equilibrium condition thus reduces to

$$\alpha_k\rho_k\frac{\mathrm{d}B_k}{\mathrm{d}\alpha_k} - P_k = \alpha_j\rho_j\frac{\mathrm{d}B_j}{\mathrm{d}\alpha_j} - P_j, \quad k \neq j. \tag{2.21}$$

The *granular* pressure is defined by

$$\beta_k = \alpha_k\rho_k\frac{\mathrm{d}B_k}{\mathrm{d}\alpha_k}. \tag{2.22}$$

From that definition, the *configuration* energy is deduced:

$$B_k = \int_{\alpha_k^0}^{\alpha_k}\frac{\beta_k}{\alpha\rho_k}\,\mathrm{d}\alpha. \tag{2.23}$$

With these notations, the equilibrium condition becomes

$$\pi_k = P_k - \beta_k = P_j - \beta_j = \pi_j, \quad \forall\, k, j, \quad k \neq j. \tag{2.24}$$

and the mixture pressure is given by

$$P = \sum_j \alpha_j P_j = \pi_k + \sum_j \alpha_j\beta_j = \pi_k + \beta \quad \text{with } \beta = \sum_j \alpha_j\beta_j. \tag{2.25}$$

The *granular* pressure (2.22), given as a function of the volume fraction, can be determined quite easily by experimental means (Kuo *et al.* 1980; Elban & Chiarito 1986). It is then necessary to find a fitting curve. Example of such a fitting function is given in Bdzil *et al.* (1999):

$$\beta_s = -\tau\left(\alpha_s - \alpha_s^0\right)\frac{\log(1-\alpha_s)}{1-\alpha_s}, \tag{2.26}$$

where the subscript s stands for the solid granular material, and τ and α_s^0 are the two given positive constant numbers.

In § 4, we will address another option with better properties regarding *granular energy* and *granular sound speed*. From now onwards, we assume that such a granular EOS is given.

To determine the volume fraction evolution equation, the mechanical equilibrium condition ($k \neq j$),

$$P_k(\rho_k, s_k) - \beta_k(\alpha_k, \rho_k) = P_j(\rho_j, s_j) - \beta_j(\alpha_j, \rho_j), \tag{2.27}$$

is differentiated along a trajectory

$$\begin{aligned} c_k^2\frac{\mathrm{d}\rho_k}{\mathrm{d}t} + \rho_k\Gamma_k T_k\frac{\mathrm{d}s_k}{\mathrm{d}t} - \frac{\beta_k}{\rho_k}\frac{\mathrm{d}\rho_k}{\mathrm{d}t} - \left(\frac{\beta_k}{\alpha_k} + \alpha_k\rho_k\frac{\mathrm{d}^2B_k}{\mathrm{d}{\alpha_k}^2}\right)\frac{\mathrm{d}\alpha_k}{\mathrm{d}t} \\ = c_j^2\frac{\mathrm{d}\rho_j}{\mathrm{d}t} + \rho_j\Gamma_j T_j\frac{\mathrm{d}s_j}{\mathrm{d}t} - \frac{\beta_j}{\rho_j}\frac{\mathrm{d}\rho_j}{\mathrm{d}t} - \left(\frac{\beta_j}{\alpha_j} + \alpha_j\rho_j\frac{\mathrm{d}^2B_j}{\mathrm{d}{\alpha_j}^2}\right)\frac{\mathrm{d}\alpha_j}{\mathrm{d}t}. \end{aligned} \tag{2.28}$$

https://doi.org/10.1017/S0022112010003794 Published online by Cambridge University Press

With the help of entropy and mass evolution equations, it is reduced to

$$\left(\frac{\rho_k c_k^2}{\alpha_k} + \alpha_k \rho_k \frac{\mathrm{d}^2 B_k}{\mathrm{d}{\alpha_k}^2}\right) \frac{\mathrm{d}\alpha_k}{\mathrm{d}t} + \left(\rho_k c_k^2 - \beta_k\right) \frac{\partial u}{\partial x} = \left(\frac{\rho_j c_j^2}{\alpha_j} + \alpha_j \rho_j \frac{\mathrm{d}^2 B_j}{\mathrm{d}{\alpha_j}^2}\right) \frac{\mathrm{d}\alpha_j}{\mathrm{d}t} + \left(\rho_j c_j^2 - \beta_j\right) \frac{\partial u}{\partial x}. \quad (2.29)$$

On the other hand, the saturation constraint reads

$$\frac{\mathrm{d}\alpha_1}{\mathrm{d}t} + \frac{\mathrm{d}\alpha_2}{\mathrm{d}t} + \cdots + \frac{\mathrm{d}\alpha_N}{\mathrm{d}t} = 0, \quad (2.30)$$

where subscript N denotes the total number of phases. Resolution of system (2.29)–(2.30) results in evolution equations for the volume fractions

$$\frac{\mathrm{d}\alpha_k}{\mathrm{d}t} = -\frac{\alpha_k}{\rho_k C_k^2}\left(\left(\rho_k c_k^2 - \beta_k\right) - \rho C^2 \sum_l \frac{\alpha_k}{\rho_k C_k^2}\left(\rho_k c_k^2 - \beta_k\right)\right) \frac{\partial u}{\partial x} \quad (2.31)$$

with

$$C_k^2 = c_k^2 + \alpha_k^2 \frac{\mathrm{d}^2 B_k}{\mathrm{d}{\alpha_k}^2} \quad \text{and} \quad \frac{1}{\rho C^2} = \sum_k \frac{\alpha_k}{\rho_k C_k^2}. \quad (2.32)$$

2.1. *Summary*

The mechanical equilibrium model thus reads as

$$\left.\begin{aligned} &\frac{\mathrm{d}\alpha_k}{\mathrm{d}t} = -\frac{\alpha_k}{\rho_k C_k^2}\left(\left(\rho_k c_k^2 - \beta_k\right) - \rho C^2 \sum_j \frac{\alpha_j}{\rho_j C_j^2}\left(\rho_j c_j^2 - \beta_j\right)\right) \frac{\partial u}{\partial x}, \\ &\frac{\partial (\alpha\,\rho)_k}{\partial t} + \frac{\partial ((\alpha\,\rho)_k\, u)}{\partial x} = 0, \\ &\frac{\partial (\rho u)}{\partial t} + \frac{\partial \left(\rho u^2 + P\right)}{\partial x} = 0, \\ &\frac{\partial (\rho E)}{\partial t} + \frac{\partial ((\rho E + P)\, u)}{\partial x} = 0, \end{aligned}\right\} \quad (2.33)$$

where the granular pressure β_k is defined by (2.22), the mechanical equilibrium condition is given by (2.24) and the mixture pressure P is given by (2.25). The total energy E is defined by

$$E = (e + B) + \frac{1}{2} u^2 \quad \text{with } e + B = \sum_k Y_k\, (e_k + B_k). \quad (2.34)$$

Finally, C_k^2 and C^2 are given by

$$C_k^2 = c_k^2 + \alpha_k^2 \frac{\mathrm{d}^2 B_k}{\mathrm{d}{\alpha_k}^2}, \quad \frac{1}{\rho C^2} = \sum_k \frac{\alpha_k}{\rho_k C_k^2}. \quad (2.35)$$

2.2. *Sound speed*

We now focus on propagation of acoustic waves in such mechanical equilibrium mixtures. This is also an important point regarding the hyperbolic properties of the governing equations. To determine the wave propagation speed, let us write the

https://doi.org/10.1017/S0022112010003794 Published online by Cambridge University Press

pressure evolution equation:

$$\frac{\mathrm{d}P}{\mathrm{d}t} = \frac{\mathrm{d}P_k}{\mathrm{d}t} - \frac{\mathrm{d}\beta_k}{\mathrm{d}t} + \sum_j \left(\frac{\mathrm{d}\alpha_j}{\mathrm{d}t}\beta_j + \alpha_j \frac{\mathrm{d}\beta_j}{\mathrm{d}t} \right)$$
$$= c_k^2 \frac{\mathrm{d}\rho_k}{\mathrm{d}t} - \frac{\beta_k}{\rho_k}\frac{\mathrm{d}\rho_k}{\mathrm{d}t} - \left(\frac{\beta_k}{\alpha_k} + \alpha_k \rho_k \frac{\mathrm{d}^2 B_k}{\mathrm{d}{\alpha_k}^2} \right) \frac{\mathrm{d}\alpha_k}{\mathrm{d}t}$$
$$+ \sum_j \left[\frac{\mathrm{d}\alpha_j}{\mathrm{d}t}\beta_j + \alpha_j \left(\frac{\beta_j}{\rho_j}\frac{\mathrm{d}\rho_j}{\mathrm{d}t} + \left(\frac{\beta_j}{\alpha_j} + \alpha_j \rho_j \frac{\mathrm{d}^2 B_j}{\mathrm{d}{\alpha_j}^2} \right) \frac{\mathrm{d}\alpha_j}{\mathrm{d}t} \right) \right]. \quad (2.36)$$

By using mass and volume fraction equations (2.31) and after some rearrangements, we get

$$\frac{\mathrm{d}P}{\mathrm{d}t} + \left[\rho C^2 \left(\sum_j \frac{\alpha_j}{\rho_j C_j^2} \left(\rho_j c_j^2 - \beta_j \right) \right)^2 - \sum_j \left(\frac{\alpha_j \left(\rho_j c_j^2 - \beta_j \right)^2}{\rho_j C_j^2} - \alpha_j \rho_j c_j^2 \right) \right] \frac{\partial u}{\partial x} = 0. \quad (2.37)$$

The square sound speed

$$C_W^2 = C^2 \left(\sum_j \frac{\alpha_j}{\rho_j C_j^2} \left(\rho_j c_j^2 - \beta_j \right) \right)^2 - \frac{1}{\rho} \sum_j \left(\frac{\alpha_j \left(\rho_j c_j^2 - \beta_j \right)^2}{\rho_j C_j^2} - \alpha_j \rho_j c_j^2 \right) \quad (2.38)$$

corresponds to the equilibrium sound speed in the granular medium. In absence of granular pressure ($\beta_j = 0$), it corresponds to the well-known non-monotonic sound speed (Wood 1930). System (2.33) is thus hyperbolic with characteristic speeds u, $u + C_W$ and $u - C_W$.

2.3. *Thermodynamic closure*

From the pure phase EOS, the mixture energy definition, the mixture pressure and mechanical equilibrium conditions, there is no difficulty to determine the mixture EOS. For the sake of simplicity, we take the example of compressible materials governed by the stiffened gas EOS. This EOS is quite accurate for description of gases, liquids and solids. The method that follows is not restricted to this example: Mie Gruneïsen-type EOS can be considered as well, or any other type of convex EOS. With the stiffened gas EOS, the energy, density and pressure are linked by the relation

$$\rho_k e_k = \frac{P_k + \gamma_k P_{k,\infty}}{\gamma_k - 1}, \quad (2.39)$$

where γ_k and $P_{k,\infty}$ are some given positive constant parameters, determined by using material reference curves. Usually, Hugoniot curves are used, but saturation curves can also be used for special purposes (Le Métayer, Massoni & Saurel 2004). The mixture internal energy reads as

$$\rho(e + B) = \sum_k \alpha_k \rho_k (e_k + B_k). \quad (2.40)$$

Inserting (2.39) in (2.40) gives us

$$\rho(e + B) - \sum_k \frac{\alpha_k \gamma_k P_{k,\infty}}{\gamma_k - 1} - \sum_k \alpha_k \rho_k B_k = \sum_k \frac{\alpha_k P_k}{\gamma_k - 1}. \quad (2.41)$$

https://doi.org/10.1017/S0022112010003794 Published online by Cambridge University Press

Now using the mixture pressure definition (2.25) and the mechanical equilibrium condition (2.24), we get

$$P = P_k - \beta_k + \sum_j \alpha_j \beta_j. \tag{2.42}$$

Inserting this relation in (2.41), we get

$$\rho e - \sum_k \frac{\alpha_k \gamma_k P_{k,\infty k}}{\gamma_k - 1} - \sum_k \alpha_k \rho_k B_k = \left(P - \sum_k \alpha_k \beta_k \right) \sum_k \frac{\alpha_k}{\gamma_k - 1} + \sum_k \frac{\alpha_k \beta_k}{\gamma_k - 1}. \tag{2.43}$$

Consequently, the mixture EOS is obtained:

$$P = \frac{\rho\,(e + B) - \sum_k \left(\dfrac{\alpha_k\,(\gamma_k P_{k,\infty} + \beta_k)}{\gamma_k - 1} \right) - \sum_k (\alpha_k \rho_k B_k)}{\sum_k \left(\dfrac{\alpha_k}{\gamma_k - 1} \right)} + \sum_k \alpha_k \beta_k. \tag{2.44}$$

System (2.33) is now closed by (2.44). This mechanical equilibrium model is able to describe wave propagation in granular mixtures. However, it is unable to reproduce compaction irreversibility. To reach this goal, we are going to build a non-equilibrium model with relaxation that will tend in some limit to system (2.33). The mechanical equilibrium model will be used during the loading process only, and unloading will be treated by the non-equilibrium model presented below.

3. Non-equilibrium model

The non-equilibrium model must involve two main features:

(*a*) the non-equilibrium model must tend to the mechanical equilibrium one when mechanical relaxation effects are stiff;

(*b*) the non-equilibrium sound speed must be greater than the equilibrium one as it is usually the case for the non-equilibrium models.

On this basis, the following model is proposed. It is an extension of the model given by Saurel *et al.* (2009) for fluid–fluid interfaces to the case of granular mixtures:

$$\left.\begin{aligned}
&\frac{\mathrm{d}\alpha_1}{\mathrm{d}t} = \mu(\pi_1 - \pi_2),\\
&\frac{\partial(\alpha\rho)_k}{\partial t} + \frac{\partial((\alpha\rho)_k\, u)}{\partial x} = 0, \quad (k = 1, 2),\\
&\frac{\partial((\alpha\rho)_1\,(e + B)_1)}{\partial t} + \frac{\partial((\alpha\rho)_1\,(e + B)_1\, u)}{\partial x} + (\alpha P)_1 \frac{\partial u}{\partial x} = -\pi_I\, \mu(\pi_1 - \pi_2),\\
&\frac{\partial((\alpha\rho)_2\,(e + B)_2)}{\partial t} + \frac{\partial((\alpha\rho)_2\,(e + B)_2\, u)}{\partial x} + (\alpha P)_2 \frac{\partial u}{\partial x} = \pi_I\, \mu(\pi_1 - \pi_2),\\
&\frac{\partial(\rho u)}{\partial t} + \frac{\partial(\rho u^2 + P)}{\partial x} = 0,\\
&\frac{\partial(\rho E)}{\partial t} + \frac{\partial((\rho E + P)\, u)}{\partial x} = 0
\end{aligned}\right\} \tag{3.1}$$

https://doi.org/10.1017/S0022112010003794 Published online by Cambridge University Press

with

$$\left.\begin{aligned} &\pi_k = P_k - \beta_k, \quad \pi_I = \frac{Z_2\pi_1 + Z_1\pi_2}{Z_1 + Z_2}, \\ &E_k = e_k + B_k + \frac{1}{2}u^2, \quad E = \sum_k Y_k E_k, \quad P = \sum_k \alpha_k P_k. \end{aligned}\right\} \tag{3.2}$$

The interfacial generalized pressure π_I has been estimated through the Riemann problem solution as in Saurel, Gavrilyuk & Renaud (2003), with the acoustic impedance $Z_k = \rho_k c_k$. One main point of this model relies on the relaxation parameter μ:

$$\mu = \begin{cases} +\infty & \text{if } \pi_1 > \pi_2, \\ 0 & \text{otherwise.} \end{cases} \tag{3.3}$$

It is implicit in this formulation that $k=1$ corresponds to the solid phase and $k=2$ to the gas phase. Thus, during loading the weak compressibility of the solid will imply $\pi_1 > \pi_2$ and a stiff pressure relaxation coefficient will be used. As it is shown in Appendix A, such a treatment is equivalent to the direct resolution of the equilibrium model given by system (2.33). During unloading a vanishing relaxation coefficient will be used.

The non-equilibrium model thus contains two limit models, the mechanical equilibrium model when the relaxation parameter tends to infinity, and a frozen model when this parameter is zero. It is necessary to analyse these two models, as it is also important to examine the physical meaning of the relaxation parameter μ as a function of π_1 and π_2. This will be addressed in a specific section, after validation of the model against experimental results. Before that, let us check the accordance of the model with the fundamental principles of thermodynamics.

3.1. *Energy conservation*

System (3.1) contains three energy equations. Two of them are the evolution of the phase energies, the last one is the mixture energy conservation. Consequently this system is overdetermined but still compatible. Numerical resolution of interface problems with fluid–fluid and fluid–granular mixture interface requires compatible overdetermined system, in particular for wave transmission. The fundamental reason is that the phase energy equations are not in conservative form. The total mixture energy equation, being conservative, guarantees the correct treatment of the two non-conservative internal energy equations in the single phase limit, i.e. on both sides of a material interface even in the presence of shocks. The mixture energy equation is thus needed for numerical reasons, as shown in Saurel *et al.* (2009).

For both theoretical and numerical reasons it is necessary to check that these three energy equations are compatible. Phase energy equations can be written in the form

$$\left.\begin{aligned} &\rho\frac{\mathrm{d}(Y_1(e+B)_1)}{\mathrm{d}t} + (\alpha P)_1\frac{\partial u}{\partial x} = -\pi_I\,\mu(\pi_1 - \pi_2), \\ &\rho\frac{\mathrm{d}(Y_2(e+B)_2)}{\mathrm{d}t} + (\alpha P)_2\frac{\partial u}{\partial x} = +\pi_I\,\mu(\pi_1 - \pi_2). \end{aligned}\right\} \tag{3.4}$$

Summing these two equations and adding the kinetic energy obtained from the mixture momentum equation, we obtain:

$$\rho\frac{\mathrm{d}}{\mathrm{d}t}\left(Y_1(e+B)_1 + Y_2(e+B)_2 + \frac{u^2}{2}\right) + \frac{\partial(u\,((\alpha P)_1 + (\alpha P)_2))}{\partial x} = 0. \tag{3.5}$$

https://doi.org/10.1017/S0022112010003794 Published online by Cambridge University Press

This last equation corresponds to the mixture energy equation presented previously in system (3.1).

3.2. *Entropy inequality*

It is important to show that the non-equilibrium model is in agreement with the entropy inequality. Let us consider the internal energy equation for phase 1, the calculations being symmetric for phase 2. It reads

$$\frac{\partial((\alpha\rho)_1\,(e+B)_1)}{\partial t}+\frac{\partial((\alpha\rho)_1\,(e+B)_1\,u)}{\partial x}+(\alpha P)_1\,\frac{\partial u}{\partial x}=-\pi_I\,\mu(\pi_1-\pi_2). \tag{3.6}$$

An equivalent form is

$$(\alpha\rho)_1\,\frac{\mathrm{d}e_1}{\mathrm{d}t}+(\alpha P)_1\,\frac{\partial u}{\partial x}=-(\pi_I+\beta_1)\,\mu(\pi_1-\pi_2). \tag{3.7}$$

With the help of the volume fraction and mass conservation equations of phase 1, the velocity divergence can be expressed as

$$\frac{\partial u}{\partial x}=-\frac{1}{\alpha_1}\,\frac{\mathrm{d}\alpha_1}{\mathrm{d}t}-\frac{1}{\rho_1}\,\frac{\mathrm{d}\rho_1}{\mathrm{d}t}=-\frac{1}{\rho_1}\,\frac{\mathrm{d}\rho_1}{\mathrm{d}t}-\frac{1}{\alpha_1}\,\mu(\pi_1-\pi_2). \tag{3.8}$$

The internal energy equation now reads

$$(\alpha\rho)_1\,\frac{\mathrm{d}e_1}{\mathrm{d}t}-\frac{(\alpha P)_1}{\rho_1}\,\frac{\mathrm{d}\rho_1}{\mathrm{d}t}=-(\pi_I+\beta_1)\,\mu(\pi_1-\pi_2)+P_1\,\mu(\pi_1-\pi_2). \tag{3.9}$$

With the help of the Gibbs identity for phase 1, we get

$$(\alpha\rho T)_1\,\frac{\mathrm{d}s_1}{\mathrm{d}t}=-(\pi_I-\pi_1)\,\mu(\pi_1-\pi_2). \tag{3.10}$$

Using the interface pressure definition for π_I given in (3.2), the entropy equation now becomes

$$(\alpha\rho T)_1\,\frac{\mathrm{d}s_1}{\mathrm{d}t}=\frac{Z_1}{Z_1+Z_2}\,\mu(\pi_1-\pi_2)^2; \tag{3.11}$$

and we get, for phase 2

$$(\alpha\rho T)_2\,\frac{\mathrm{d}s_2}{\mathrm{d}t}=\frac{Z_2}{Z_1+Z_2}\,\mu(\pi_1-\pi_2)^2. \tag{3.12}$$

Since each phase has clearly a non-negative entropy production, the mixture entropy evolution is guaranteed to be non-negative.

3.3. *Frozen model*

During the unloading stage, the relaxation parameter is set to zero ($\mu=0$). It is interesting to examine the acoustic properties of the corresponding model, as the hysteresis phenomenon shown in figure 1 is expected to be reproduced by the change in acoustic behaviour when μ varies from $+\infty$ to 0.

The frozen limit model corresponds to system (3.1) when $\mu=0$. An alternative formulation of this system is

$$\frac{\partial \boldsymbol{W}}{\partial t}+\boldsymbol{A}(\boldsymbol{W})\,\frac{\partial \boldsymbol{W}}{\partial x}=0, \tag{3.13}$$

https://doi.org/10.1017/S0022112010003794 Published online by Cambridge University Press

with the vector of variables $\boldsymbol{W} = (\alpha_1,\ s_1,\ s_2,\ u,\ p_1,\ p_2)^{\mathrm{T}}$, and the matrix $\boldsymbol{A}$ defined by

$$\boldsymbol{A}(\boldsymbol{W}) = \begin{pmatrix} u & 0 & 0 & 0 & 0 & 0 \\ 0 & u & 0 & 0 & 0 & 0 \\ 0 & 0 & u & 0 & 0 & 0 \\ (p_1 - p_2)/\rho & 0 & 0 & u & \alpha_1/\rho & \alpha_2/\rho \\ 0 & 0 & 0 & \rho_1 c_1^2 & u & 0 \\ 0 & 0 & 0 & \rho_2 c_2^2 & 0 & u \end{pmatrix}. \tag{3.14}$$

The eigenvalues of this matrix correspond to the wave speeds

$$\lambda_0 = u, \qquad \lambda_1 = u - c_f, \qquad \lambda_2 = u + c_f. \tag{3.15}$$

Here, the frozen sound speed c_f is defined by

$$c_f^2 = Y_1 c_1^2 + Y_2 c_2^2. \tag{3.16}$$

This sound speed is much greater than the mechanical equilibrium sound speed given in (2.38), as shown in Appendix B. Moreover, this result guarantees hyperbolicity of the non-equilibrium model (3.1).

3.4. *Limit system when $\mu \to +\infty$*

During compression the relaxation parameter is assumed stiff ($\mu \to +\infty$). It is important to show that the asymptotic limit when $\mu \to +\infty$ of the non-equilibrium model corresponds to the mechanical equilibrium one (2.33). This is detailed in Appendix A. Thus, it is now clear that formulation (3.1) contains two limit models, each one being hyperbolic and having its own mixture sound speed. Closure of this model is achieved by defining appropriate EOS and relaxation parameter μ. Equations of state are proposed in the next section. Justification of the relaxation parameter switch will be examined in § 7.

4. Equations of state

Since a powder compaction situation involves two thermodynamic phases (solid and gas), three EOS are needed. Indeed, both materials being compressible, an EOS for each phase is needed to express its thermodynamic behaviour. This is particularly important as we are dealing with large-amplitude wave dynamics. A third EOS is needed to express inter-granular pressure linked to its corresponding configuration energy.

4.1. *Thermodynamic equations of state*

For the sake of simplicity, each material is assumed to obey the *stiffened gas* EOS. This formulation is able to deal with both gas and condensed phases. It reads as

$$P_k = (\gamma_k - 1)\,\rho_k e_k - \gamma_k P_{k,\infty}. \tag{4.1}$$

Parameters γ_k and $P_{k,\infty}$ are characteristic of a given material. They are determined from a given reference curve, in general the experimental Hugoniot curve, as detailed for example in Le Métayer *et al.* (2004). Data for some materials are given in table 1.

4.2. *Granular equation of state*

When dealing with solid–gas mixtures, only the solid phase is subjected to inter-granular efforts and contains consequently configurational energy. The granular EOS

https://doi.org/10.1017/S0022112010003794 Published online by Cambridge University Press

	$\rho_0\,(\mathrm{kg\,m^{-3}})$	γ	$p_\infty\,(\mathrm{Pa})$
Air	1	1.4	0
Liquid water	1000	4.4	6×10^8
HMX (octogen: cyclotetramethylene–tetranitramine)	1903	5.5	31×10^8
NaCl	2165	4.2	63×10^8

TABLE 1. Stiffened gas EOS data for some materials under interest for powder compaction.

is determined by quasi-static compression of powders. The system volume is measured, and the granular bed solid volume fraction is deduced, as a function of the applied stress. This type of experiment is described, for example, in Kuo *et al.* (1980), Elban & Chiarito (1986) and more recently in Jogi (2003), where successive loading–unloading cycles have been studied.

The granular EOS is a simple way to express complex multi-dimensional effects occurring at grains scale such as rearrangements and plastic deformations by using experimental data quite easy to obtain. With this approach microscopic effects are summarized in *granular* pressure and energy with the help of macroscopic variables only.

It is possible to fit (granular pressure – solid volume fraction α) curves by the following function, representing the configuration energy (the granular pressure will be determined subsequently):

$$B(\alpha)=\begin{cases}B_a(\alpha) & \text{if } \alpha_0<\alpha<1,\\ 0 & \text{otherwise,}\end{cases} \tag{4.2}$$

where

$$B_a(\alpha)=a[(1-\alpha)\,\log(1-\alpha)+(1+\log(1-\alpha_0))(\alpha-\alpha_0)-(1-\alpha_0)\log(1-\alpha_0)]^n. \tag{4.3}$$

The positive parameter α_0 corresponds to the solid volume fraction when the granular pressure is zero. This volume fraction depends on the powder material, on its morphology, on its granulometry, etc. It is clear in (4.2)–(4.3) that $B(\alpha_0)=0$.

Parameters a and n are also characteristic of a given powder, and more precisely of its response during quasi-static loading.

For the present model, it is necessary to formulate the first and second derivatives of $B(\alpha)$ defined by (4.2)–(4.3). The first derivative reads as

$$\frac{\mathrm{d}B}{\mathrm{d}\alpha}=\begin{cases}B_a'(\alpha)=-an(\log(1-\alpha)+1)\left(\dfrac{B(\alpha)}{a}\right)^{(n-1)/n} & \text{if } \alpha_0<\alpha<1,\\ 0 & \text{otherwise.}\end{cases} \tag{4.4}$$

Obviously,

$$\frac{\mathrm{d}B}{\mathrm{d}\alpha}(\alpha_0)=0,\quad \text{when } n>1. \tag{4.5}$$

This guarantees tangency of the pressure curve with the volume fraction axis at $\alpha=\alpha_0$. The granular pressure is readily deduced from:

$$\beta_k=(\alpha\rho)_k\,\frac{\mathrm{d}B_k}{\mathrm{d}\alpha_k}. \tag{4.6}$$

https://doi.org/10.1017/S0022112010003794 Published online by Cambridge University Press

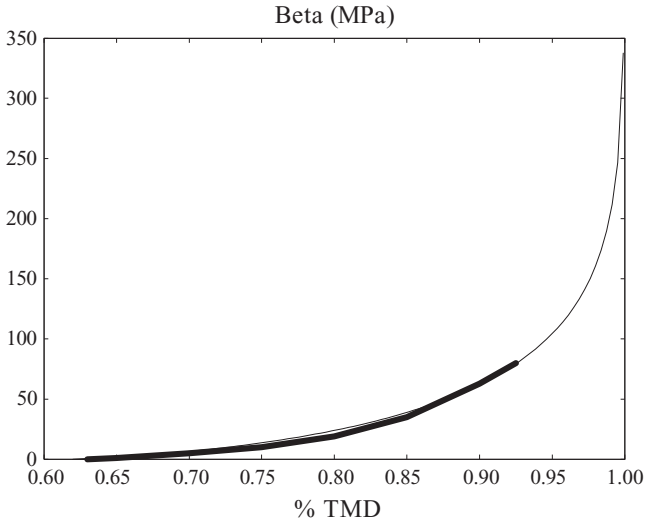


FIGURE 2. Approximation of the experimental compression curve (bold lines) for granular HMX following Jogi (2003) by the granular EOS (4.2)–(4.6) in lines. The fitting parameters are determined in the zone where the curves are superimposed. Function behaviour for extrapolated data is shown when solid volume fraction tends to one. Obviously, compressible effects involved in the thermodynamic EOS become important in this range. Fitting parameters in the solid volume fraction range 0.63–0.93 are $a = 3 \times 10^4$ Pa and $n = 1.1$. The percentage of theoretical maximum density is defined by % TMD $= (\alpha_s \rho_s)/\rho_{s0}$.

Then, the second derivative is determined, as it is involved in the solid-phase sound speed definition:

$$\frac{\mathrm{d}^2 B}{\mathrm{d}\alpha^2} = \begin{cases} B_a''(\alpha) & \text{if } \alpha_0 < \alpha < 1, \\ 0 & \text{otherwise,} \end{cases} \tag{4.7}$$

where

$$B_a''(\alpha) = an \left[\left(\frac{1}{1-\alpha} \right) \left(\frac{B(\alpha)}{a} \right)^{(n-1)/n} + (n-1)\,(\log(1-\alpha)+1)^2 \left(\frac{B(\alpha)}{a} \right)^{(n-2)/n} \right]. \tag{4.8}$$

By using Jogi (2003) experimental data, based on granular HMX, with particle size around 100 µm, we have obtained the fitting curve in lines shown on figure 2, on the basis of definition (4.6) with configuration energy defined by (4.2)–(4.3).

Using Duberg & Nyström (1986) experiments based on granular NaCl, we have obtained the results shown in figure 3. We now have all data to perform the model's numerical validation for wave dynamics in powders and study compaction hysteresis phenomenon. Appropriate numerical schemes have been derived in Saurel *et al.* (2009) in a simplified situation of fluid–fluid model. The same algorithm can be used for the present application, except regarding some details which are specified in the following section.

5. Numerical method

The non-equilibrium model (3.1) is close to the two-phase model studied in Saurel *et al.* (2009). The numerical method described in that paper proceeds in three main steps:

https://doi.org/10.1017/S0022112010003794 Published online by Cambridge University Press

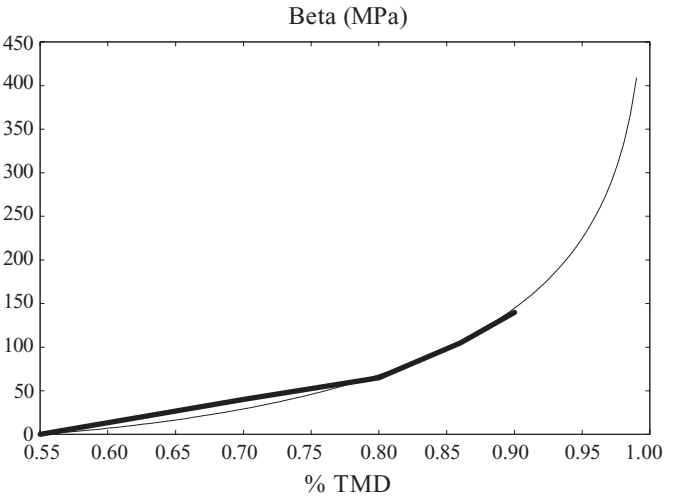


FIGURE 3. Approximation of the experimental compression curve (bold lines) for granular NaCl following Duberg & Nyström (1986) by the granular EOS (4.2)–(4.6) in lines. The fitting parameters are determined in the zone, where the curves are superimposed. Function behaviour for extrapolated data is shown when solid volume fraction tends to one. Obviously, compressible effects involved in the thermodynamic EOS become important in this range. Fitting parameters in the solid volume fraction range 0.55–0.9 are $a = 5 \times 10^4$ Pa and $n = 1.02$ (% TMD $= (\alpha_s \rho_s)/\rho_{s0}$).

(*a*) hyperbolic step: solve the non-equilibrium system without relaxation terms;

(*b*) relaxation step: determine the equilibrium pressure and associated volume fraction;

(*c*) internal energies reset: use the equilibrium volume fraction in the mixture EOS, based on mixture energy conservation (2.44), determine the corrected equilibrium pressure and reset the phase internal energy.

In the present context of granular materials, the formulation solved in the hyperbolic step is the following ($k = 1, 2$):

$$\left.\begin{aligned}
&\frac{\partial \alpha_1}{\partial t} + u\,\frac{\partial \alpha_1}{\partial x} = 0,\\
&\frac{\partial (\alpha\rho)_k}{\partial t} + \frac{\partial ((\alpha\rho)_k\, u)}{\partial x} = 0,\\
&\frac{\partial ((\alpha\rho)_k e_k)}{\partial t} + \frac{\partial ((\alpha\rho)_k e_k u)}{\partial x} + (\alpha P)_k\,\frac{\partial u}{\partial x} = 0,\\
&\frac{\partial (\rho u)}{\partial t} + \frac{\partial \left(\rho u^2 + (\alpha P)_1 + (\alpha P)_2\right)}{\partial x} = 0,\\
&\frac{\partial (\rho E)}{\partial t} + \frac{\partial ((\rho E + (\alpha_1 P_1 + \alpha_2 P_2))\, u)}{\partial x} = 0.
\end{aligned}\right\} \tag{5.1}$$

The only difference compared to the formulation used in Saurel *et al.* (2009) for fluid mixtures is in the total mixture energy definition ($E = e + B + u^2/2$) that involves a thermodynamic part and a granular one. The internal energy equations of formulation (3.1) are simplified in (5.1) with the help of the granular Gibbs identity (2.22).

https://doi.org/10.1017/S0022112010003794 Published online by Cambridge University Press

The third step of this method (internal energy reset) is also unchanged. The only change is related to the mixture EOS (2.44) that is used instead of its fluid variant.

The second step (pressure relaxation) is, however, quite different as the mechanical equilibrium condition is different too. This relaxation step is done only if $\pi_1 > \pi_2$.

The relaxation step consists in solving the differential system:

$$\left.\begin{aligned}
&\frac{\partial \alpha_1}{\partial t} = \mu(\pi_1 - \pi_2),\\
&\frac{\partial (\alpha\rho)_k}{\partial t} = 0,\\
&\frac{\partial ((\alpha\rho)_1 (e+B)_1)}{\partial t} = -\pi_I\, \mu(\pi_1 - \pi_2),\\
&\frac{\partial ((\alpha\rho)_2 (e+B)_2)}{\partial t} = +\pi_I\, \mu(\pi_1 - \pi_2),\\
&\frac{\partial (\rho u)}{\partial t} = 0,\\
&\frac{\partial (\rho E)}{\partial t} = 0
\end{aligned}\right\} \tag{5.2}$$

in the limit $\mu \to +\infty$ and with π_I defined by (3.2).

Since only the equilibrium solution is required, the aim is to replace this ordinary differential system by an algebraic one. After some manipulations, the internal energy equations become ($k = 1, 2$):

$$\frac{\partial (e_k + B_k)}{\partial t} + \pi_I \frac{\partial v_k}{\partial t} = 0. \tag{5.3}$$

Under integral form, this system becomes

$$(e_k + B_k) - \left(e_k^0 + B_k^0\right) + \hat{\pi}_{I,k}\left(v_k - v_k^0\right) = 0 \tag{5.4}$$

with

$$\hat{\pi}_{I,k} = \frac{1}{v_k - v_k^0} \int_0^{\Delta t} \pi_I \frac{\partial v_k}{\partial t}\, \mathrm{d}t. \tag{5.5}$$

Following Saurel *et al.* (2009), the interfacial pressure average can be estimated with sufficient accuracy by setting $\hat{\pi}_{I,k} = \pi$, which represents the pressure in the equilibrium state.

The system to solve is thus composed of the following equations:

$$e_k(P, v_k) + B_k(\alpha_k, \rho_k) - e_k^0\left(P_k^0, v_k^0\right) - B_k\left(\alpha_k^0, \rho_k^0\right) + \pi\left(v_k - v_k^0\right) = 0, \quad k = 1, 2. \tag{5.6}$$

The apparent densities $(\alpha\rho)_k$ remain constant during the relaxation process. Also, the volume fractions can be expressed as $\alpha_k = (\alpha\rho)_k^0\, v_k$. Consequently, system (5.6) becomes ($k = 1, 2$)

$$e_k(P, v_k) + B_k(v_k) - e_k^0\left(P_k^0, v_k^0\right) - B_k\left(v_k^0\right) + \pi\left(v_k - v_k^0\right) = 0. \tag{5.7}$$

This system involves three unknowns v_k ($k = 1, 2$) and the equilibrium pressure π. Its closure is achieved by the saturation condition

$$\sum_k \alpha_k = 1. \tag{5.8}$$

https://doi.org/10.1017/S0022112010003794 Published online by Cambridge University Press

It is more convenient to express this condition as

$$\sum_k (\alpha\rho)_k v_k = 1. \tag{5.9}$$

To be more explicit, let us take the example of materials governed by the stiffened gas EOS (4.1). The internal energy in (5.6) can be replaced by a function of pressure and specific volume

$$e_k = v_k \frac{P_k + \gamma_k P_{k,\infty}}{\gamma_k - 1}. \tag{5.10}$$

The pressures in each phase can be expressed with the help of the equilibrium stress as functions of π, $P_k = \pi + \beta_k(\alpha_k, \rho_k)$. System (5.6) becomes

$$\frac{\pi + \beta_k + \gamma_k P_{k,\infty}}{\gamma_k - 1} v_k + B_k - \frac{P_k^0 + \gamma_k P_{k,\infty k}}{\gamma_k - 1} v_k^0 - B_k^0 + \pi\left(v_k - v_k^0\right) = 0. \tag{5.11}$$

Note that in state '0', corresponding to the state at the end of the hyperbolic step, the equilibrium pressure π has not been used, as this state is out of mechanical equilibrium.

After some manipulations, we get

$$v_k = \frac{\left(P_k^0 + \gamma_k\, P_{k,\infty} + (\gamma_k - 1)\,\pi\right) v_k^0 + (\gamma_k - 1)\left(B_k^0 - B_k\right)}{\beta_k + \gamma_k\,(\pi + P_{k,\infty k})}. \tag{5.12}$$

As this equation involves functions $\beta_k(\alpha_k, \rho_k)$ and $B_k(\alpha_k, \rho_k)$ that can be rewritten as $\beta_k(v_k)$ and $B_k(v_k)$, the preceding equation becomes a function to be solved for the determination of specific volume v_k. For a given estimate of the equilibrium pressure π, specific volumes v_k are the solutions of this equation. The pressure estimate is correct if the constraint (5.9) is fulfilled. The Newton method is appropriate for such a task.

6. Test problems and validations

The model has been built to deal with three main features: irreversibility of powder compaction, wave dynamics (shock and expansion waves) and computation of interfaces separating fluids and granular mixtures. The model's ability to simulate these various phenomena is validated on several test problems.

6.1. *Compaction of a powder sample*

Let us consider a HMX powder sample 1.5 cm long, made of the same powder as those studied by Jogi (2003) with an initial solid volume fraction of 0.63. The sample is pressed by a left-moving piston at imposed velocity of 1 m s^{-1} to the right. The right wall boundary is at rest and assumed to be indeformable. The situation is depicted in figure 4.

The computational domain involves 100 cells. The method described in the preceding section is used with an extended version on moving meshes. The corresponding solution is shown at times 25.5 µs, 51.0 µs and 76.4 µs in figure 5.

The propagation mechanism shown in figure 5 is very fast compared to the piston motion. Multiple reflections occur between the two boundaries during slow piston motion rendering the various variable fields quasi-uniform, functions only of time.

With the same piston velocity, the powder sample is pressed up to the solid volume fraction of 0.80, then the piston is removed at very slow velocity (−0.01 m s^{-1}), until the mixture pressure reaches the atmospheric one. At this moment, the piston motion

https://doi.org/10.1017/S0022112010003794 Published online by Cambridge University Press

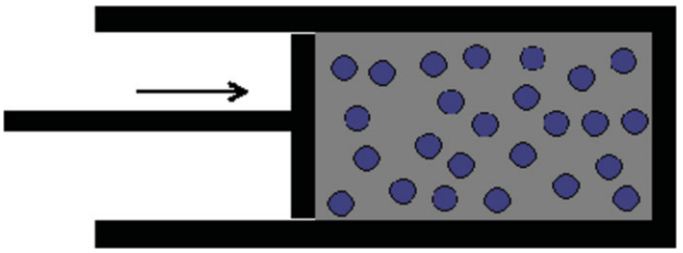


FIGURE 4. (Colour online) Schematic representation of a powder press.

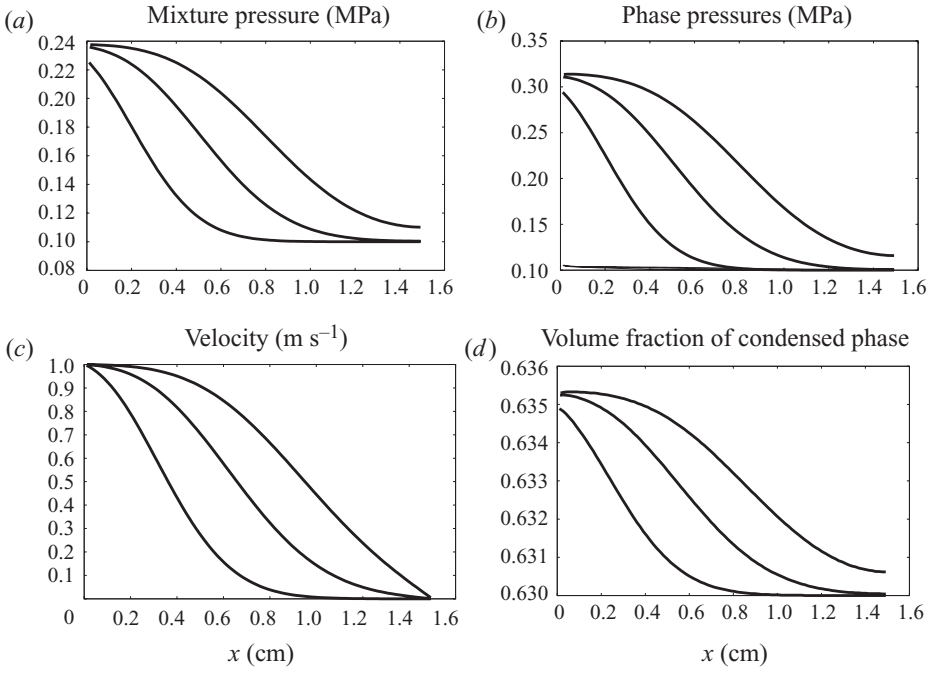


FIGURE 5. Propagation of a weak compaction wave in the mixture. Mixture pressure ($P = \alpha_1 P_1 + \alpha_2 P_2$), phase pressures, mixture velocity and solid volume fraction profiles are shown at times 25.5 μs, 51.0 μs and 76.4 μs. The compression wave is dispersed and produces a weak solid volume fraction increase. The pressure difference between the gas phase (bottom lines) and solid phase (solid lines) due to the granular pressure is visible on the second graph. The compaction wave reflects on the tube end at the last instant. Stiff pressure relaxation is used, corresponding to the mechanical equilibrium model.

is stopped. Flow variables being uniform in space only their time evolution is shown in figure 6.

The first graph of figure 6 shows piston evolution. Its velocity is positive initially, then it is negative for about 1.5 ms, and zero when the mixture pressure reaches atmospheric one. Piston trajectory is shown on the second graph. The mixture pressure increases during compression, then decreases rapidly when the piston has negative velocity, even if this velocity is very low. This is a consequence of the sound speed change in the model, which ranges from the mechanical equilibrium one when $\mu \to +\infty$ to the frozen one when $\mu = 0$. The solid volume fraction increases during compression and remains frozen during expansion. Thus, the granular medium stays compact. The thermodynamic solid pressure has the same evolution as the mixture

https://doi.org/10.1017/S0022112010003794 Published online by Cambridge University Press

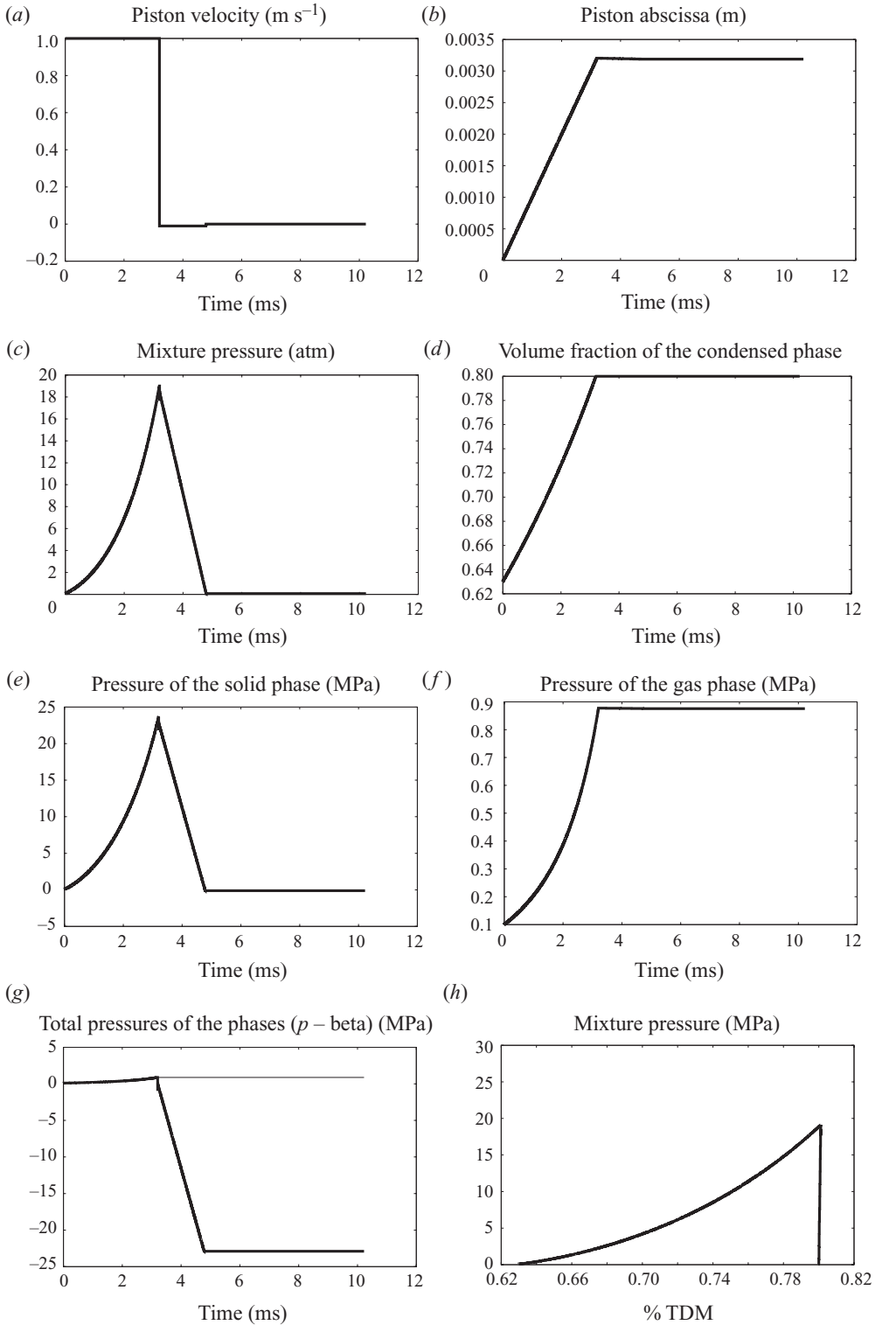


FIGURE 6. Evolution of flow variables versus time for a loading–unloading cycle with HMX powder. The maximum solid volume fraction of 80 % is reached at time 3 ms and remains unchanged during unloading. The hysteresis cycle is shown on the last graph.

https://doi.org/10.1017/S0022112010003794 Published online by Cambridge University Press

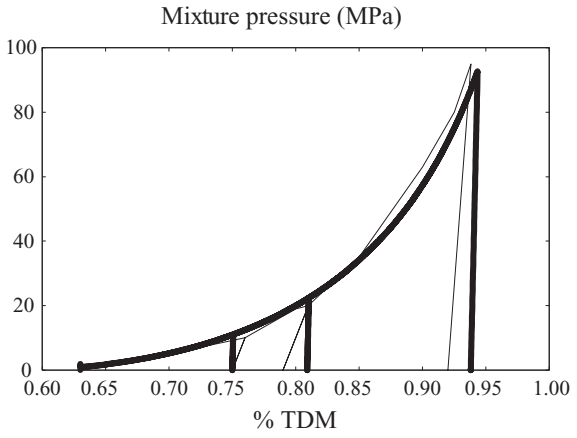


FIGURE 7. Mixture pressure evolution as a function of compression rate (% TMD $= \alpha_s \rho_s / \rho_s^0$) for three successive loading–unloading cycles of HMX powder. Experimental data are shown in thin lines, numerical results in bold lines. The agreement is very good for a model free of adjustable parameter.

pressure that decreases abruptly during expansion. The solid phase thus recovers atmospheric pressure at the cycle end. Contrarily, the gas phase stays compressed in pores, as the sixth graph shows. The graph of *total pressures* ($P_k - \beta_k$) shows stress equality during compression stage and disequilibrium created during expansion stage. This disequilibrium is not surprising. At the cycle end the solid pressure has reached atmospheric one, but the granular pressure β_s that represents the effect of plastic stress at the granular scale is still present. To end, the most characteristic graph is the last one, where the mixture pressure is shown as a function of the compression rate (% TMD $= (\alpha_s \rho_s)/\rho_{s0}$, where ρ_{s0} represents the standard density of the solid phase). The compression rate exhibits a slight decrease during expansion, due to the mixture compressibility. Indeed, the expansion curve around 80 % TMD is not strictly vertical. This last graph clearly shows the ability of the model to predict the compaction hysteresis phenomenon.

We now address the same experiments as done by Jogi (2003), with three successive loading–unloading cycles. In these examples, the volume fraction has been recorded at the end of each unloading stage. For the first cycle, the powder is pressed up to the solid volume fraction of 0.75, and then the stress is relaxed. Then the same sample is compressed again, up to the solid volume fraction of 0.809 and the stress relaxed again. For the third cycle, the mixture is pressed up to the solid volume fraction of 0.938 and the stress relaxed again. Results are given in figure 7 and compared to Jogi (2003) experimental data.

Similar agreement is obtained with Gonthier (2003, 2004) model when compared to Jogi (2003) experimental results. However, the two-phase flow model of Gonthier contains explicitly an extra function corresponding to no-load solid volume fraction. This function needs extra experimental efforts for model's calibration.

In order to show the ability of the present model to deal with different kinds of powders, we now consider NaCl powder, studied experimentally by Duberg & Nyström (1986). EOS parameters are given in table 1 and figure 3. A comparison between model predictions and experiments is shown in figure 8.

We now examine the model's ability to deal with large-amplitude wave propagation as well as interfaces separating pure fluids and granular mixtures.

https://doi.org/10.1017/S0022112010003794 Published online by Cambridge University Press

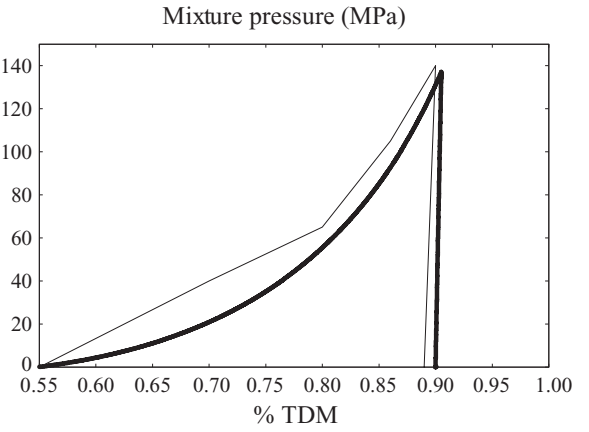


FIGURE 8. Mixture pressure evolution as a function of compression rate for NaCl powder. Experimental data are shown in thin lines, numerical results in bold lines.

6.2. *Waves and interfaces dynamics*

In all following tests, the granular material corresponds to HMX powder with EOS parameters given in table 1 and figure 2.

Let us consider a *shock tube* of 1 m length involving a high-pressure chamber on the left, filled with a gas at the initial pressure of (0.1 GPa), and a low-pressure chamber on the right, filled with the same granular material as the one studied in figures 5–7 at atmospheric pressure. The gas is governed by the ideal gas EOS with air polytropic coefficient. An initial volume fraction discontinuity is thus present in the tube at abscissa 0.5 m. In order to prevent division by zero in the flow model, the solid volume fraction in the left chamber is set to 10^{-6}. In the right chamber, it is set to 0.63. The initial density of solid is constant in the whole domain and equal to $1903\,\mathrm{kg\,m^{-3}}$. That of the gas phase in the high-pressure chamber is set to $100\,\mathrm{kg\,m^{-3}}$ while in the right chamber it is set to $1\,\mathrm{kg\,m^{-3}}$. Both initial states are initially at rest. The aim of this test problem is to show the model's ability to compute right facing shock and associated bed compaction, left facing expansion wave and the interface evolution separating the nearly pure gas from a granular mixture. Results are shown in figure 9 at time 0.38 ms. The mesh involves 1000 cells.

On the first graph of figure 9, the left facing expansion wave and right facing shock are clearly visible. At the interface location, visible on the fourth graph, the pressure and velocity are perfectly continuous. The phase pressure graph shows the solid pressure in lines and the gas pressure in dash lines. There is a pressure difference between these two phase pressures, due to the granular pressure effect. On the left, the solid pressure reaches a very low level and is not in equilibrium with the gas phase, as the left part of the domain corresponds to an expansion process. This has no consequence as the solid volume fraction in this zone is very small.

The same test is rerun with increased initial gas pressure in the left chamber by a factor 100 (10 GPa) in order to simulate conditions close to detonation product contact with granular media. Corresponding results are shown in figure 10 at time 36 μs.

This test shows the ability of the model to deal with interfaces separating fluids and granular mixtures in severe conditions, where fluid behaviour of granular materials is recovered as a limit. Pressure difference between phases in the granular bed becomes negligible.

https://doi.org/10.1017/S0022112010003794 Published online by Cambridge University Press

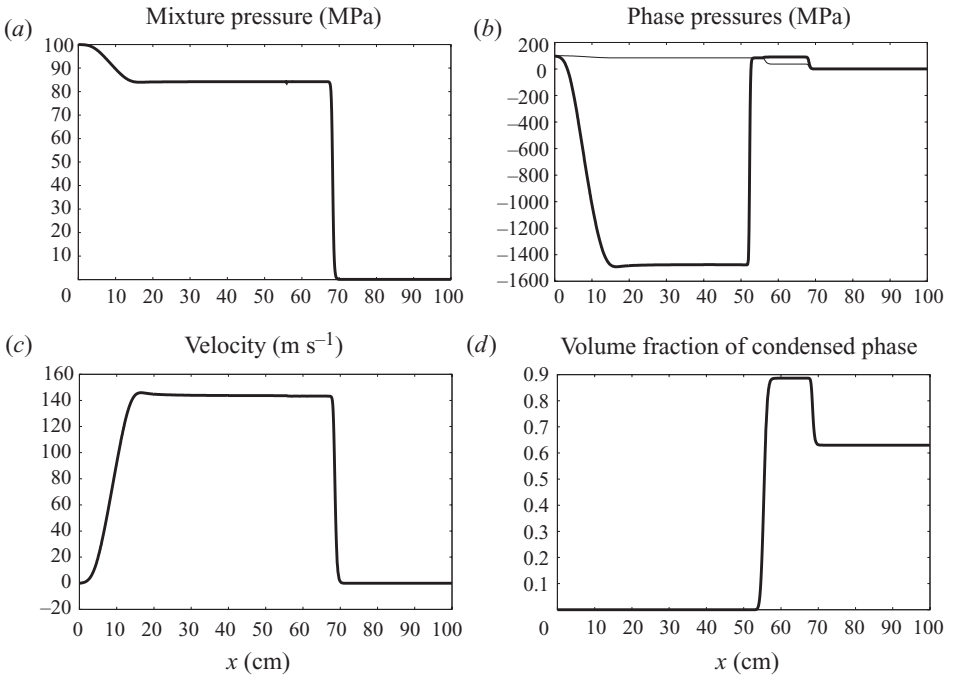


FIGURE 9. *Shock tube* with high-pressure gas on the left and granular mixture on the right. Interface conditions of equal mixture pressure and equal velocities are perfectly matched. The granular mixture is compacted by the shock wave.

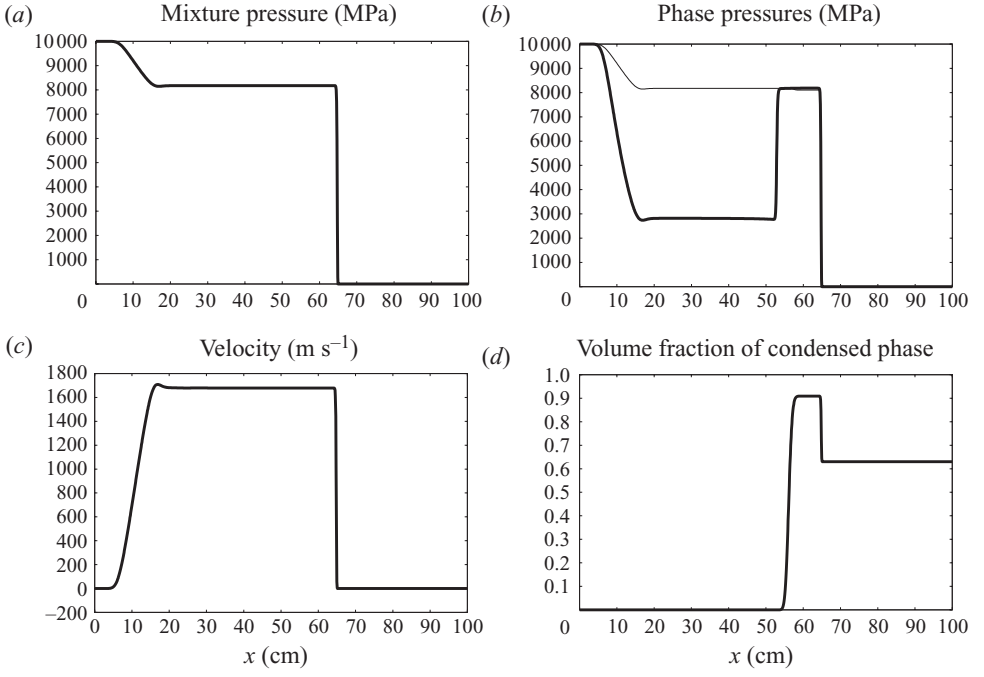


FIGURE 10. *Shock tube* with high-pressure gas on the left and granular mixture on the right. Interface conditions of equal mixture pressure and equal velocities are again perfectly matched. The pressure difference between phases in the compacted zone in the right chamber now vanishes, showing negligible effects of granular pressure in these conditions, at least regarding wave dynamics. The fluid limit is recovered.

https://doi.org/10.1017/S0022112010003794 Published online by Cambridge University Press

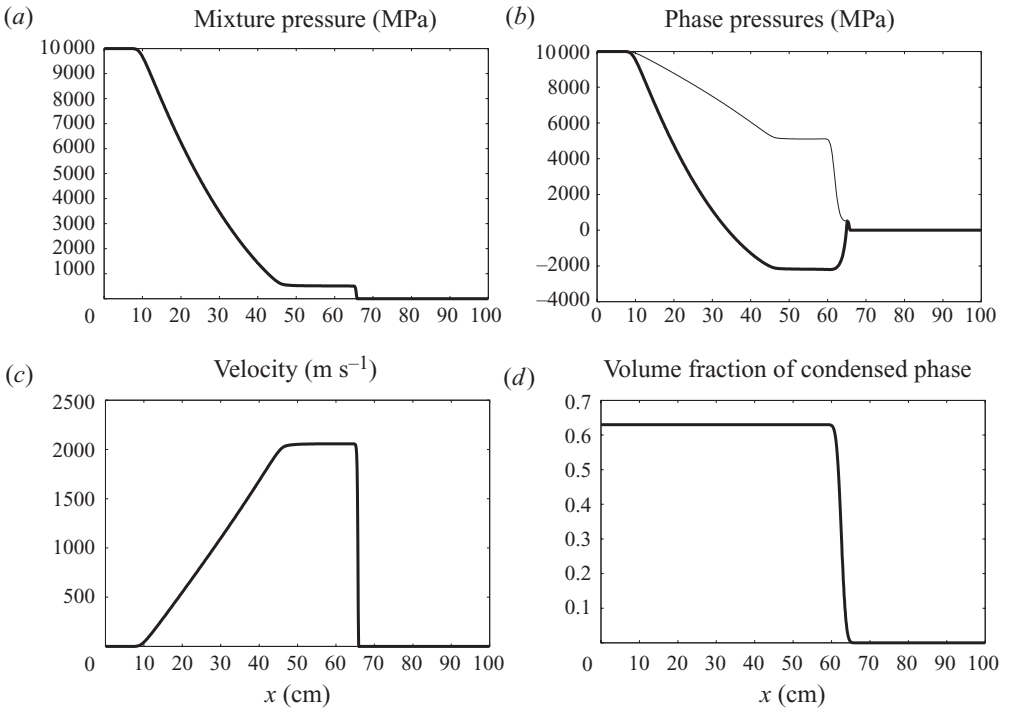


FIGURE 11. *Shock tube* with high-pressure granular mixture on the left and low-pressure gas on the right. Interface conditions of equal mixture pressure and equal velocities are again perfectly matched even in the absence of relaxation effect ($\mu = 0$).

We now consider the symmetric situation with the expansion of a high-pressure granular bed. In the left chamber, the granular bed is at the initial pressure of 10 GPa. On the right, gas is present at atmospheric pressure. In these conditions, the model uses a zero relaxation parameter ($\mu = 0$) and its ability to solve interfaces has to be checked. This is the goal of the results shown in the figure 11.

These various tests show the model's capabilities to deal with various kinds of interface problems:

(i) when the granular bed is in compression, corresponding to the use of the model with stiff relaxation ($\mu \to +\infty$) in compaction zones;

(ii) when the granular bed is under expansion, corresponding to the use of the frozen non-equilibrium model ($\mu = 0$) to express the irreversible character of powder compaction.

Both limit models are suitable for interface problem computations.

6.3. *Two-dimensional examples*

Both model and method are able to deal with complex multi-dimensional phenomena appearing during the impact and penetration of a projectile into a granular bed. This is illustrated by an example given in figure 12, where a solid projectile (considered as non-deformable) impacts a granular mixture. The solid projectile is made of copper ($\rho = 8900\,\mathrm{kg\,m^{-3}}$), and moves to the right at the initial velocity of $10\,\mathrm{m\,s^{-1}}$.

The copper projectile has an initial radius of 0.1 m. The other dimensions are given in figure 12. The same HMX powder as previously studied is considered, with the initial HMX density of $1903\,\mathrm{kg\,m^{-3}}$. The granular bed has an initial solid volume

https://doi.org/10.1017/S0022112010003794 Published online by Cambridge University Press

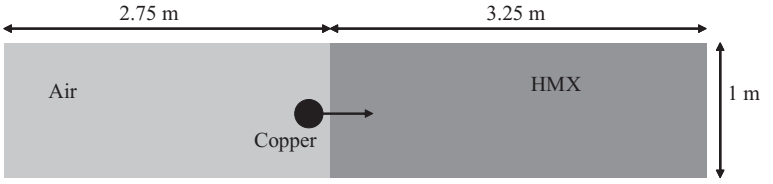


FIGURE 12. Schematic representation of the initial conditions during the impact of a copper projectile into a granular mixture made of HMX powder with an initial solid volume fraction of 0.63.

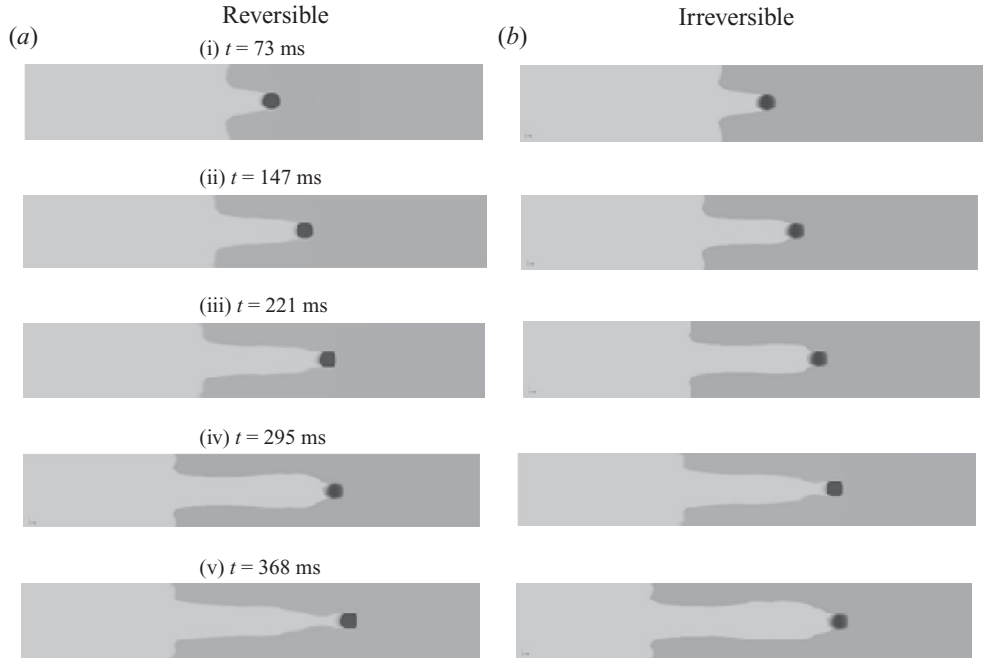


FIGURE 13. Qualitative flow behaviour during the impact of a solid projectile into a granular bed. On the left graph column, the mechanical equilibrium model has been solved by the help of the non-equilibrium one, which corresponds to using stiff relaxation parameter everywhere ($\mu \to +\infty$). On the right graph column, the switch (3.3) is used, which corresponds to irreversible compaction. Computed results are shown at times (*a*) $t = 73$ ms, (*b*) $t = 147$ ms, (*c*) $t = 221$ ms, (*d*) $t = 295$ ms and (*e*) $t = 368$ ms.

fraction of 0.63. The surrounding air, as well as the air contained in the powder, has the initial density of $1\,\mathrm{kg\,m^{-3}}$.

The flow behaviour is clearly different in figure 13 when irreversibility is accounted for, especially in the projectile wake. This can be important for example for the determination of the amount of ejected powder due to projectile impact.

This type of computation involves three materials: the air, the granular powder and the solid projectile. Model and method extension to an arbitrary number of phases is straightforward. The non-deformable character of the solid is solved with the correction procedure detailed in Petitpas *et al.* (2009).

6.4. *Shock-induced powder compaction*

We now examined model's validity against experimental data for shock propagation in powder samples. Corresponding experiments have been done by Sandusky & Liddiard

https://doi.org/10.1017/S0022112010003794 Published online by Cambridge University Press

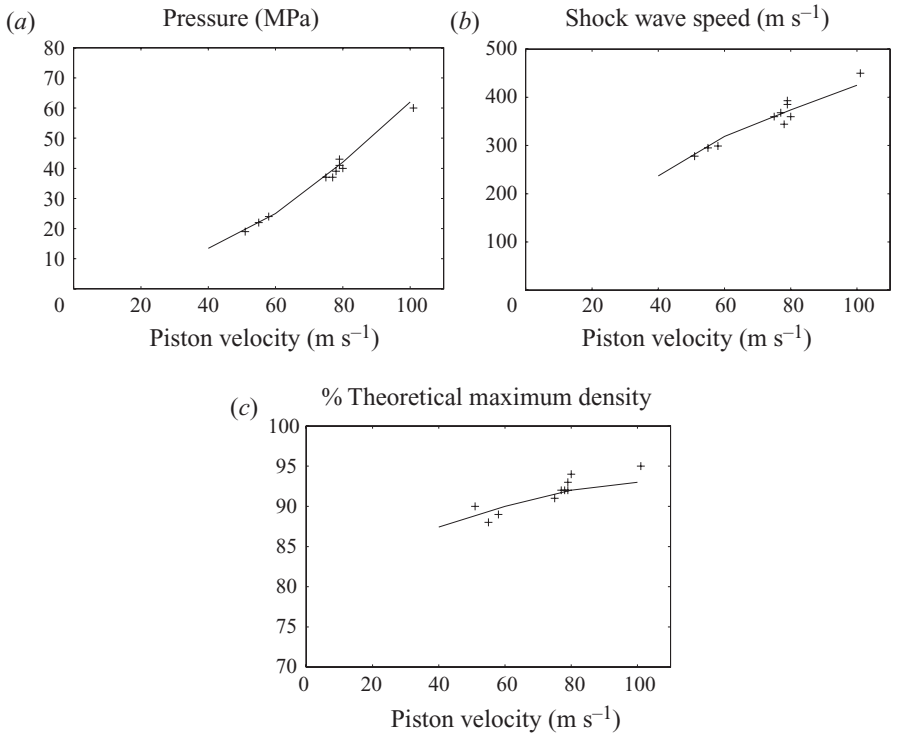


FIGURE 14. Comparison of numerical (lines) and experimental (symbol) results for waves speeds, pressure and per cent theoretical maximum density in the shocked state for various piston impact velocities.

(1985). In the following test case, the granular material corresponds to HMX powder with the following parameters $\alpha_{s0} = 0.73$, $a = 10^4$ and $n = 1.05$ for the granular EOS.

Thermodynamics HMX parameters are those of table 1. We assume the porosity to be filled with air with density $\rho = 1.2\,\mathrm{kg\,m^{-3}}$ and $\gamma = 1.4$. At initial time, the HMX-air mixture is at rest and a piston impacts the granular bed at various velocities. In the figure 14, we compare experimental measurements (cross symbols) and numerical results (lines). The shock wave speed, the shock pressure and the per cent theoretical maximum density after compaction for various piston velocities are presented. The results are in excellent agreement.

7. Relaxation parameter switch discussion

The non-equilibrium model (3.1) is able to link in a unique formulation, the frozen model with sound speed $c_f^2 = Y_1 c_1^2 + Y_2 c_2^2$, when $\mu = 0$, and the mechanical equilibrium model (2.33), with sound speed (2.38) when $\mu \to +\infty$. The irreversible powder compaction cycle shown in figure 1 has thus been successfully reproduced in figures 7 and 8 with the following relaxation parameter switch

$$\mu = \begin{cases} +\infty, & \text{if } \pi_1 > \pi_2, \\ 0, & \text{otherwise.} \end{cases} \tag{7.1}$$

To explain this switch procedure, it is first important to agree with the idea this function is a simplification of a certainly much more complex function, which remains to be determined, equations (7.1) being a fair approximation for most flow situations.

https://doi.org/10.1017/S0022112010003794 Published online by Cambridge University Press

It seems that powder compaction involves at least four different stages:

(*a*) *Stress accumulation.* During the early events of granular bed compaction, acoustic wave propagate and reflect on the solid piston and wall boundaries making the mixture pressure increase, in particular those of the solid phase. Elastic deformations appear, but are of low amplitude due to the high resistance of elastic bodies to deformation. During this stage, the solid volume fraction is nearly constant, and the pressure relaxation parameter is close to zero. But for slightly increasing compression rates (a few per cent) the stress differential $(\pi_1-\pi_2)$ exceeds the plastic limit Y_p. For HMX, this limit is of the order of 100 MPa (Khasainov *et al.* 1981). Then, the process undergoes plastic deformation.

(*b*) *Plastic deformation.* Plastic deformations result in stress relaxation, i.e. $\pi_1=\pi_2$ at the end of the relaxation process. This process occurs obviously at finite rate, but if the details of this relaxation process are not of interest, and if only the equilibrium state has importance, the relaxation parameter can be set stiff ($\mu\to+\infty$). During this stage, plastic stresses increase, as well as the granular pressure β_s that summarizes their effects. It is important to remind that this relaxation process occurring in plastic regime is irreversible.

(*c*) *Frozen unloading*. Plastic stresses around gas pores are now present and are represented by β_s. If the piston is removed, the solid pressure rapidly adjusts to the external one (atmospheric for example), but the plastic stresses at pore scales remain present and unchanged. Plastic deformation being irreversible, pore volumes are unchanged, as well as solid volume fraction. This corresponds to the use of the frozen model ($\mu=0$). The granular bed remains compact and out of equilibrium.

(*d*) *Long time relaxation.* If the compact granular solid is left in these non-equilibrium conditions for a very long time (several months or years), stress relaxation will occur, producing compact solid dislocation.

Our goal is not to model the (*a*) and (*d*) stages. To illustrate stages (*a*) and (*b*) let us consider again the same granular HMX sample under *frozen* compression, corresponding to the *stress accumulation* stage, followed by finite rate relaxation step corresponding to *plastic deformation.* During the second stage, the relaxation parameter is arbitrarily set to $\mu=10^{-6}\,\mathrm{Pa}^{-1}\,\mathrm{s}^{-1}$. The powder sample is compressed by a relative volume of 1 % only. To illustrate the scale of this transformation, stages (*a*) and (*b*) are shown on the same graph as experimental data in figure 15.

During stage (*a*), the mixture pressure increases dramatically as the volume fraction is frozen and the solid is weakly compressible. Considering $\mu=0$ in stage (*a*) is certainly excessive, but it shows that the plastic limit of 100 MPa for HMX can be overpassed easily (the stress differential at the spike value is $\pi_1-\pi_2=180$ MPa). Then plastic relaxation occurs and the mixture pressure decreases dramatically, to reach finally the equilibrium curve.

As the equilibrium curve has been reached after plastic deformations, which are obviously irreversible, the unloading stage (*c*) will occur at constant solid volume fraction. This justifies the use of $\mu=0$ during unloading stage (*c*).

In most practical applications, there is no need to describe the details of stages (*a*) and (*b*). Only the equilibrium relaxed state of stage (*b*) is needed. This is done by using $\mu\to+\infty$ instead of stages (*a*) and (*b*). This justifies switch (7.1). This switch procedure makes the model free of adjustable parameter.

The main limitation with this model relies in its single velocity description of multiphase mixtures. In some applications, gas (or liquid) permeation in granular beds may have important effects. To deal with these effects, the preceding model

https://doi.org/10.1017/S0022112010003794 Published online by Cambridge University Press

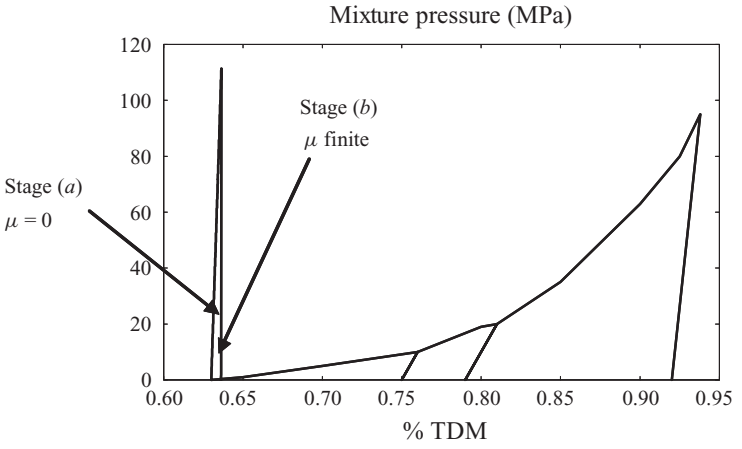


FIGURE 15. Decomposition of stages (*a*) and (*b*) of the compaction process. The plastic limit is exceeded during stage (*a*), even for very low relative volume compression, and stress relaxation occurs in stage (*b*). These events are shown in bold lines. The end state of the relaxation path belongs to the equilibrium curve of the considered material (experimental results in lines).

needs important and difficult extension: restoration of velocity drift effects. This issue is addressed in the following section.

8. Compaction model with velocity drift effects

The compaction model presented before is a temperature non-equilibrium two-phase flow model with a single velocity. In specific situations, fluid permeation effects in granular beds may have importance. Following Guillard & Duval (2007), a Darcy-type law can be obtained to model drift effects. This Darcy law was obtained on the basis of asymptotic analysis of the velocity non-equilibrium Baer & Nunziato (1986) model in the barotropic case. We extend here the approach to non-barotropic fluids in the presence of configuration (granular) effects.

8.1. *Non-equilibrium model*

The Baer & Nunziato (1986) model considers each phase as compressible, evolving with its own velocity, temperature and pressure. The system is hyperbolic and involves seven partial differential equations for two phases in one dimension. Its natural generalization to the case of granular mixtures in absence of heat and mass transfers is (here only the equations for phase $k = 1$ are written down)

$$\left.\begin{aligned}
&\frac{\partial \alpha_1}{\partial t} + u_I \frac{\partial \alpha_1}{\partial x} = \mu \pi_R, \\
&\frac{\partial (\alpha\rho)_1}{\partial t} + \frac{\partial (\alpha\rho u)_1}{\partial x} = 0, \\
&\frac{\partial (\alpha\rho u)_1}{\partial t} + \frac{\partial (\alpha\rho u^2 + \alpha P)_1}{\partial x} = \pi_I \frac{\partial \alpha_1}{\partial x} - \lambda u_R, \\
&\frac{\partial (\alpha\rho E)_1}{\partial t} + \frac{\partial (\alpha(\rho E + P)u)_1}{\partial x} = \pi_I u_I \frac{\partial \alpha_1}{\partial x} - \lambda u'_I u_R - \mu \pi_I \pi_R.
\end{aligned}\right\} \tag{8.1}$$

https://doi.org/10.1017/S0022112010003794 Published online by Cambridge University Press

Here, $\pi_R = (\pi_1 - \pi_2)$ and $u_R = (u_1 - u_2)$ are associated to stress and velocity relaxation parameters μ and λ. Four symmetric equations are available for the second phase.

As previously, the total energy for phase k involves configuration energy:

$$E_k = e_k + B_k + \tfrac{1}{2} u_k^2. \tag{8.2}$$

Following Saurel *et al.* (2003), we define the interfacial variables by

$$\left.\begin{aligned} u_I &= u_I' - \operatorname{sgn}\left(\frac{\partial \alpha_1}{\partial x}\right) \frac{\pi_R}{Z_1 + Z_2}, \quad u_I' = \frac{Z_1 u_1 + Z_2 u_2}{Z_1 + Z_2}, \\ \pi_I &= \pi_I' - \operatorname{sgn}\left(\frac{\partial \alpha_1}{\partial x}\right) \frac{Z_1 Z_2}{Z_1 + Z_2} u_R, \quad \pi_I' = \frac{Z_2 \pi_1 + Z_1 \pi_2}{Z_1 + Z_2}. \end{aligned}\right\} \tag{8.3}$$

Here $Z_k = \rho_k c_k$ is the acoustic impedance of phase k. The Darcy-type law, responsible for gas penetration is obtained on the basis of asymptotic analysis of flow model (8.1) in the limit of stiff mechanical relaxation. To perform this analysis, we express system (8.1) in terms of physical variables (density, pressure, velocity). Corresponding equations are summarized hereafter:

$$\left.\begin{aligned} &\frac{\mathrm{d}_1 \alpha_1}{\mathrm{d}t} = \frac{Z_2}{Z_1 + Z_2} u_R \frac{\partial \alpha_1}{\partial x} + \mu' \pi_R, \\ &\alpha_1 \left(\frac{\mathrm{d}_1 \rho_1}{\mathrm{d}t} + \rho_1 \frac{\partial u_1}{\partial x} \right) = -\rho_1 \frac{\mathrm{d}_1 \alpha_1}{\mathrm{d}t}, \\ &(\alpha\rho)_1 \frac{\mathrm{d}_1 u_1}{\mathrm{d}t} + \alpha_1 \frac{\partial P_1}{\partial x} = -\left(\beta_1 + \frac{Z_1}{Z_1 + Z_2} \pi_R \right) \frac{\partial \alpha_1}{\partial x} - \lambda' u_R, \\ &\alpha_1 \left(\frac{\mathrm{d}_1 P_1}{\mathrm{d}t} + \rho_1 c_1^2 \frac{\partial u_1}{\partial x} \right) = -\rho_1 c_1^2 \frac{\mathrm{d}_1 \alpha_1}{\mathrm{d}t} + 2\, \Gamma_1 \frac{Z_1 Z_2}{(Z_1 + Z_2)^2} u_R \pi_R \frac{\partial \alpha_1}{\partial x} \\ &\quad + \Gamma_1 \left(\frac{Z_2}{Z_1 + Z_2} \lambda' u_R^2 + \frac{Z_1}{Z_1 + Z_2} \mu' \pi_R^2 \right), \end{aligned}\right\} \tag{8.4}$$

Here,

$$\left.\begin{aligned} &\frac{\mathrm{d}_k}{\mathrm{d}t} = \frac{\partial}{\partial t} + u_k \frac{\partial}{\partial x}, \quad k = 1,\ 2, \\ &\left.\frac{\partial e_k}{\partial P_k}\right)_{\rho_k} = \frac{1}{\rho_k \Gamma_k}, \quad \left.\frac{\partial e_k}{\partial \rho_k}\right)_{P_k} = \frac{P_k}{\rho_k} - \frac{c_k^2}{\rho_k \Gamma_k}, \\ &\mu' = \mu + \frac{1}{Z_1 + Z_2} \left| \frac{\partial \alpha_1}{\partial x} \right|, \quad \lambda' = \lambda + \frac{Z_1 Z_2}{Z_1 + Z_2} \left| \frac{\partial \alpha_1}{\partial x} \right|. \end{aligned}\right\} \tag{8.5}$$

The associated entropy balance equation reads

$$\begin{aligned} (\alpha\rho T)_1 \frac{\mathrm{d}_1 s_1}{\mathrm{d}t} = {} & \frac{Z_2}{Z_1 + Z_2} \lambda u_R^2 + \frac{Z_1}{Z_1 + Z_2} \mu \pi_R^2 \\ & + \frac{Z_1}{(Z_1 + Z_2)^2} \left| \frac{\partial \alpha_1}{\partial x} \right| \left(Z_2 u_R + \operatorname{sgn}\left(\frac{\partial \alpha_1}{\partial x}\right) \pi_R \right)^2, \end{aligned} \tag{8.6}$$

ensuring non-negative entropy production in phase 1. A symmetric result can be obtained for the second phase. Obviously, non-negative entropy production for the mixture is thus guaranteed.

https://doi.org/10.1017/S0022112010003794 Published online by Cambridge University Press

8.2. *Supplementary equations*

Combining the phase velocity equations of system (8.4), the following evolution equation for the relative velocity is readily obtained

$$\frac{\partial u_R}{\partial t} + \frac{\partial}{\partial x}\left(u_R\left(u - \frac{Y_1 - Y_2}{2}\,u_R\right)\right) = -\frac{1}{\rho Y_1 Y_2}\left(Y_2\,\frac{\partial(\alpha_1 P_1)}{\partial x} - Y_1\,\frac{\partial(\alpha_2 P_2)}{\partial x} - \pi_I'\,\frac{\partial \alpha_1}{\partial x} + \lambda'\,u_R\right). \quad (8.7)$$

This last relation is important for the determination of the Darcy-type law, around the mechanical equilibrium limit.

System (8.1) also implies the following mixture mass, mixture momentum and mixture energy conservation equations, which are obtained by summing respectively the two mass equations, the two momentum equations and the two energy equations of system (8.1). These mixture conservation laws read

$$\left.\begin{aligned} &\frac{\partial \rho}{\partial t} + \frac{\partial(\rho u)}{\partial x} = 0,\\ &\frac{\partial(\rho u)}{\partial t} + \frac{\partial\left(\rho u^2 + P + \rho Y_1 Y_2\,u_R^2\right)}{\partial x} = 0,\\ &\frac{\partial(\rho E)}{\partial t} + \frac{\partial((\rho E + P)u + \rho Y_1 Y_2\,u_R\,H_R)}{\partial x} = 0; \end{aligned}\right\} \quad (8.8)$$

where $(k = 1,\ 2)$,

$$\left.\begin{aligned} &\rho = \alpha_1\rho_1 + \alpha_2\rho_2, \quad P = \alpha_1 P_1 + \alpha_2 P_2,\\ &u = Y_1 u_1 + Y_2 u_2, \quad Y_k = (\alpha\rho)_k/\rho,\\ &E = Y_1(e_1 + B_1) + Y_2(e_2 + B_2) + \frac{1}{2}\left(u^2 + Y_1 Y_2 u_R^2\right), \quad H_k = E_k + \frac{P_k}{\rho_k},\\ &H_R = H_1 - H_2, \quad u_R = (u_1 - u_2), \end{aligned}\right\} \quad (8.9)$$

respectively define the mixture mass, pressure, velocity, phase k mass fraction, mixture total energy, phase k total enthalpy, phase total enthalpy difference and phase velocity difference.

The term $(Y_1 Y_2 u_R^2)/2$ represents a *turbulent* energy due to relative motion and the term $\rho Y_1 Y_2 u_R^2$ represents the associated *turbulent* pressure. There is no assumption made in system (8.7). *Turbulent* terms appear just as a consequence of the relative velocity consideration.

With these notations, the mass equations of each phase can be written as

$$\left.\begin{aligned} &\frac{\partial(\alpha\rho)_1}{\partial t} + \frac{\partial((\alpha\rho)_1 u)}{\partial x} + \frac{\partial(\rho Y_1 Y_2 u_R)}{\partial x} = 0,\\ &\frac{\partial(\alpha\rho)_2}{\partial t} + \frac{\partial((\alpha\rho)_2 u)}{\partial x} - \frac{\partial(\rho Y_1 Y_2 u_R)}{\partial x} = 0, \end{aligned}\right\} \quad (8.10)$$

8.3. *Asymptotic analysis*

The asymptotic analysis presented in this section follows the lines of Kapila *et al.* (2001). Each flow variable is assumed to be smooth enough to possess the asymptotic expansion $f = f^0 + \varepsilon f^1$ where f^0 represents the mechanical equilibrium state and f^1

https://doi.org/10.1017/S0022112010003794 Published online by Cambridge University Press

a small perturbation. Inversely, the mechanical relaxation parameters are supposed to be stiff, namely

$$\left.\begin{aligned} \mu' &= \frac{\mu_0}{\varepsilon}, \quad \mu_0 = \text{cte} > 0, \\ \lambda' &= \frac{\lambda_0}{\varepsilon}, \quad \lambda_0 = \text{cte} > 0. \end{aligned}\right\} \tag{8.11}$$

Inserting these definitions in (8.4), the following mechanical equilibrium constraints are obtained at the order $1/\varepsilon$

$$\left.\begin{aligned} &\pi_1^0 = \pi_2^0, \\ &u_R^0 = 0, \quad \text{or} \quad u_1^0 = u_2^0 = u^0. \end{aligned}\right\} \tag{8.12}$$

The Darcy-type law is obtained at the zero order expansion of the relative velocity equation (8.7)

$$\lambda_0 u_R^1 = Y_1^0 \frac{\partial (\alpha P)_2^0}{\partial x} - Y_2^0 \frac{\partial (\alpha P)_1^0}{\partial x} + \pi^0 \frac{\partial \alpha_1^0}{\partial x}. \tag{8.13}$$

With the help of (8.12) and mixture pressure definition, it can be rewritten as

$$u_R^1 = \frac{1}{\lambda_0} \left(\left(\alpha_1^0 - Y_1^0\right) \frac{\partial P^0}{\partial x} - \alpha_2^0 \frac{\partial (\alpha\beta)_1^0}{\partial x} + \alpha_1^0 \frac{\partial (\alpha\beta)_2^0}{\partial x} \right). \tag{8.14}$$

The relative velocity thus reads

$$u_R = u_R^0 + \varepsilon u_R^1 = \frac{1}{\lambda} \left(\left(\alpha_1^0 - Y_1^0\right) \frac{\partial P^0}{\partial x} - \alpha_2^0 \frac{\partial (\alpha\beta)_1^0}{\partial x} + \alpha_1^0 \frac{\partial (\alpha\beta)_2^0}{\partial x} \right). \tag{8.15}$$

Finally, omitting superscripts '0', we can formulate the following flow model with permeation effects

$$\left.\begin{aligned} &\frac{\partial (\alpha\rho)_1}{\partial t} + \frac{\partial ((\alpha\rho)_1 u)}{\partial x} + \frac{\partial (\rho Y_1 Y_2 u_R)}{\partial x} = 0, \\ &\frac{\partial (\alpha\rho)_2}{\partial t} + \frac{\partial ((\alpha\rho)_2 u)}{\partial x} - \frac{\partial (\rho Y_1 Y_2 u_R)}{\partial x} = 0, \\ &\frac{\partial (\rho u)}{\partial t} + \frac{\partial (\rho u^2 + P)}{\partial x} = 0, \\ &\frac{\partial (\rho E)}{\partial t} + \frac{\partial ((\rho E + P) u + \rho Y_1 Y_2 u_R H_R)}{\partial x} = 0, \end{aligned}\right\} \tag{8.16}$$

with

$$\left.\begin{aligned} u_R &= \frac{1}{\lambda} \left((\alpha_1 - Y_1) \frac{\partial P}{\partial x} - \alpha_2 \frac{\partial (\alpha\beta)_1}{\partial x} + \alpha_1 \frac{\partial (\alpha\beta)_2}{\partial x} \right), \quad \pi_1 = \pi_2, \\ E &= Y_1 (e_1 + B_1) + Y_2 (e_2 + B_2) + \frac{1}{2} u^2, \quad P = \alpha_1 P_1 + \alpha_2 P_2. \end{aligned}\right\} \tag{8.17}$$

The *turbulent pressure* $(\rho Y_1 Y_2 u_R^2)$ and *turbulent energy* $((Y_1 Y_2 u_R^2)/2)$ terms have disappeared, as a consequence of the mechanical equilibrium constraints (8.12). However, this system is not closed, as temperature disequilibrium is present. Closure of this system requires an appropriate volume fraction equation that should be determined in agreement with the entropy inequality. This is the aim of the following subsection.

https://doi.org/10.1017/S0022112010003794 Published online by Cambridge University Press

8.4. *Volume fraction and entropy equations*

The method developed in Saurel *et al.* (2008) to determine the volume fraction equation consists in determining the entropy equations from a system composed of

(i) the mixture internal energy equation written in terms of entropy and volume fraction evolutions. Such an equation is obtained from the system of conservation laws (8.16)–(8.17);

(ii) the mechanical equilibrium condition ($\pi_1 = \pi_2$), differentiated along a trajectory, linking the same entropy and volume fraction evolutions.

From this system, the entropy equations are obtained as a function of volume fraction evolution equations. Analysis of the entropy production terms provides information to determine the volume fraction equation, in agreement with the mixture entropy inequality.

8.4.1. *Energy conservation constraint*

Let us examine the mixture energy equation. Combination of mass, momentum and energy equation of system (8.26) yields to the following equation:

$$\frac{\mathrm{d}\mathscr{E}}{\mathrm{d}t} + P\frac{\mathrm{d}v}{\mathrm{d}t} + \frac{1}{\rho}\frac{\partial(\rho Y_1 Y_2 u_R\,((h+B)_1 - (h+B)_2))}{\partial x} = 0, \tag{8.18}$$

where the mixture internal energy $\mathscr{E}$, the specific volume v of the mixture and the mixture pressure P are respectively given by

$$\mathscr{E} = Y_1(e+B)_1 + Y_2(e+B)_2, \quad v = Y_1 v_1 + Y_2 v_2, \quad P = \pi + \sum_j \alpha_j \beta_j. \tag{8.19}$$

With these definitions and relation (2.22), the mixture energy equation becomes

$$Y_1 T_1 \frac{\mathrm{d}s_1}{\mathrm{d}t} + Y_2 T_2 \frac{\mathrm{d}s_2}{\mathrm{d}t} + ((h+B)_1 - (h+B)_2)\frac{\mathrm{d}Y_1}{\mathrm{d}t} + \frac{1}{\rho}\frac{\partial(\rho Y_1 Y_2 u_R\,((h+B)_1 - (h+B)_2))}{\partial x} = 0. \tag{8.20}$$

Using the phase mass equations, the energy equation thus becomes

$$Y_1 T_1 \frac{\mathrm{d}s_1}{\mathrm{d}t} + Y_2 T_2 \frac{\mathrm{d}s_2}{\mathrm{d}t} + Y_1 Y_2\, u_R \frac{\partial((h+B)_1 - (h+B)_2)}{\partial x} = 0. \tag{8.21}$$

It is worth to mention that this equation can also be written as

$$Y_1 T_1 \frac{\mathrm{d}_1 s_1}{\mathrm{d}t} + Y_2 T_2 \frac{\mathrm{d}_2 s_2}{\mathrm{d}t} + Y_1 Y_2\, u_R \left[\frac{\partial h_1}{\partial x} - T_1\frac{\partial s_1}{\partial x} - \left(\frac{\partial h_2}{\partial x} - T_2\frac{\partial s_2}{\partial x}\right) + \frac{\partial B_1}{\partial x} - \frac{\partial B_2}{\partial x}\right] = 0. \tag{8.22}$$

Noticing that for $k = 1, 2$

$$\frac{1}{\rho_k}\frac{\partial P_k}{\partial x} = \frac{\partial h_k}{\partial x} - T_k\frac{\partial s_k}{\partial x}, \quad \text{and} \quad \frac{\partial B_k}{\partial x} = \frac{\beta_k}{(\alpha\rho)_k}\frac{\partial \alpha_k}{\partial x}, \tag{8.23}$$

we obtain

$$Y_1 T_1 \frac{\mathrm{d}_1 s_1}{\mathrm{d}t} + Y_2 T_2 \frac{\mathrm{d}_2 s_2}{\mathrm{d}t} - \frac{1}{\rho}\, u_R \left[(Y_1 - \alpha_1)\frac{\partial \pi}{\partial x} - Y_2\frac{\partial(\alpha\beta)_1}{\partial x} + Y_1\frac{\partial(\alpha\beta)_2}{\partial x}\right] = 0. \tag{8.24}$$

https://doi.org/10.1017/S0022112010003794 Published online by Cambridge University Press

As the relative velocity (8.15) can also be expressed as

$$u_R = \frac{1}{\lambda}\left[(Y_1 - \alpha_1)\frac{\partial \pi}{\partial x} - Y_2 \frac{\partial(\alpha\beta)_1}{\partial x} + Y_1 \frac{\partial(\alpha\beta)_2}{\partial x}\right], \tag{8.25}$$

we get

$$Y_1 T_1 \frac{\mathrm{d}_1 s_1}{\mathrm{d}t} + Y_2 T_2 \frac{\mathrm{d}_2 s_2}{\mathrm{d}t} = \frac{\lambda}{\rho} u_R^2. \tag{8.26}$$

8.4.2. *Mechanical equilibrium constraint*

The mechanical equilibrium condition reads

$$P_1(\rho_1, s_1) - \beta_1(\rho_1, \alpha_1) = P_2(\rho_2, s_2) - \beta_2(\rho_2, \alpha_2). \tag{8.27}$$

Differentiating this equation leads to

$$\begin{aligned} &\frac{\partial P_1}{\partial \rho_1}\Big)_{s_1} \frac{\mathrm{d}\rho_1}{\mathrm{d}t} + \frac{\partial P_1}{\partial s_1}\Big)_{\rho_1} \frac{\mathrm{d}s_1}{\mathrm{d}t} - \frac{\mathrm{d}B_1}{\mathrm{d}\alpha_1}\left(\alpha_1 \frac{\mathrm{d}\rho_1}{\mathrm{d}t} + \rho_1 \frac{\mathrm{d}\alpha_1}{\mathrm{d}t}\right) \\ &\quad - (\alpha\rho)_1 \frac{\mathrm{d}^2 B_1}{\mathrm{d}{\alpha_1}^2} \frac{\mathrm{d}\alpha_1}{\mathrm{d}t} = \frac{\partial P_2}{\partial \rho_2}\Big)_{s_2} \frac{\mathrm{d}\rho_2}{\mathrm{d}t} + \frac{\partial P_2}{\partial s_2}\Big)_{\rho_2} \frac{\mathrm{d}s_2}{\mathrm{d}t} \\ &\quad - \frac{\mathrm{d}B_2}{\mathrm{d}\alpha_2}\left(\alpha_2 \frac{\mathrm{d}\rho_2}{\mathrm{d}t} + \rho_2 \frac{\mathrm{d}\alpha_2}{\mathrm{d}t}\right) - (\alpha\rho)_2 \frac{\mathrm{d}^2 B_2}{\mathrm{d}{\alpha_2}^2} \frac{\mathrm{d}\alpha_2}{\mathrm{d}t}. \end{aligned} \tag{8.28}$$

Using the definitions

$$\frac{\partial P_k}{\partial \rho_k}\Big)_{s_k} = {c_k}^2, \quad \frac{\partial P_k}{\partial s_k}\Big)_{\rho_k} = \rho_k \Gamma_k T_k, \quad \text{and} \quad C_k^2 = c_k^2 + \alpha_k^2 \frac{\mathrm{d}^2 B_k}{\mathrm{d}{\alpha_k}^2}, \tag{8.29}$$

as well as mass equations of each phase and granular pressure definition, we get

$$(\rho\Gamma T)_1 \frac{\mathrm{d}s_1}{\mathrm{d}t} - (\rho\Gamma T)_2 \frac{\mathrm{d}s_2}{\mathrm{d}t} = \left(\frac{\rho_1 C_1^2}{\alpha_1} + \frac{\rho_2 C_2^2}{\alpha_2}\right)\left(\frac{\mathrm{d}\alpha_1}{\mathrm{d}t} - \rho C_W^2 \frac{\alpha_1\alpha_2}{\rho_1 C_1^2\, \rho_2 C_2^2}\mathscr{A}\right), \tag{8.30}$$

where

$$\left.\begin{aligned} &\mathscr{A} = \big((\rho_2 c_2^2 - \beta_2) - (\rho_1 c_1^2 - \beta_1)\big)\frac{\partial u}{\partial x} + \left(\frac{\rho_1 c_1^2 - \beta_1}{(\alpha\rho)_1} + \frac{\rho_2 c_2^2 - \beta_2}{(\alpha\rho)_2}\right)\frac{\partial(\rho Y_1 Y_2 u_R)}{\partial x}, \\ &\frac{1}{\rho C_W^2} = \frac{\alpha_1}{\rho_1 C_1^2} + \frac{\alpha_2}{\rho_2 C_2^2}. \end{aligned}\right\} \tag{8.31}$$

It can also be expressed as

$$\left.\begin{aligned} &(\rho\Gamma T)_1 \frac{\mathrm{d}_1 s_1}{\mathrm{d}t} - (\rho\Gamma T)_2 \frac{\mathrm{d}_2 s_2}{\mathrm{d}t} = \left(\frac{\rho_1 C_1^2}{\alpha_1} + \frac{\rho_2 C_2^2}{\alpha_2}\right)\left(\frac{\mathrm{d}\alpha_1}{\mathrm{d}t} - \rho C_W^2 \frac{\alpha_1\alpha_2}{\rho_1 C_1^2\, \rho_2 C_2^2}\mathscr{B}\right), \\ &\mathscr{B} = \mathscr{A} + \rho Y_1 Y_2 u_R \left(\frac{\Gamma_1}{\alpha_1} T_1 \frac{\partial s_1}{\partial x} + \frac{\Gamma_2}{\alpha_2} T_2 \frac{\partial s_2}{\partial x}\right). \end{aligned}\right\} \tag{8.32}$$

Let us express this equation as

$$(\rho\,\Gamma T)_1 \frac{\mathrm{d}_1 s_1}{\mathrm{d}t} - (\rho\,\Gamma T)_2 \frac{\mathrm{d}_2 s_2}{\mathrm{d}t} = \left(\frac{\rho_1 C_1^2}{\alpha_1} + \frac{\rho_2 C_2^2}{\alpha_2}\right)\mathbb{A}. \tag{8.33}$$

https://doi.org/10.1017/S0022112010003794 Published online by Cambridge University Press

Determination of the entropy equations therefore results in solving the system composed of (8.26) and (8.32)

$$\left.\begin{aligned} Y_1 T_1 \frac{\mathrm{d}_1 s_1}{\mathrm{d}t} + Y_2 T_2 \frac{\mathrm{d}_2 s_2}{\mathrm{d}t} &= \frac{\lambda}{\rho} u_R{}^2, \\ (\rho \Gamma T)_1 \frac{\mathrm{d}_1 s_1}{\mathrm{d}t} - (\rho \Gamma T)_2 \frac{\mathrm{d}_2 s_2}{\mathrm{d}t} &= \left(\frac{\rho_1 C_1^2}{\alpha_1} + \frac{\rho_2 C_2^2}{\alpha_2} \right) \mathbb{A}, \end{aligned}\right\} \tag{8.34}$$

the solutions of which are

$$\left.\begin{aligned} (\alpha\rho)_1 \frac{\mathrm{d}_1 s_1}{\mathrm{d}t} &= \frac{\Gamma}{T_1} \frac{\alpha_1}{\Gamma_1} \left(\lambda u_R^2 + \frac{\alpha_2}{\Gamma_2} \frac{\rho_1 C_1^2}{\alpha_1} \frac{\rho_2 C_2^2}{\alpha_2} \frac{1}{\rho C_W^2} \mathbb{A} \right), \\ (\alpha\rho)_2 \frac{\mathrm{d}_2 s_2}{\mathrm{d}t} &= \frac{\Gamma}{T_2} \frac{\alpha_2}{\Gamma_2} \left(\lambda u_R^2 + \frac{\alpha_1}{\Gamma_1} \frac{\rho_1 C_1^2}{\alpha_1} \frac{\rho_2 C_2^2}{\alpha_2} \frac{1}{\rho C_W^2} \mathbb{A} \right), \end{aligned}\right\} \tag{8.35}$$

with

$$\frac{1}{\Gamma} = \frac{\alpha_1}{\Gamma_1} + \frac{\alpha_2}{\Gamma_2}. \tag{8.36}$$

Therefore, the mixture entropy equation reads

$$\begin{aligned} &\frac{\partial((\alpha\rho s)_1 + (\alpha\rho s)_2)}{\partial t} + \frac{\partial(((\alpha\rho s)_1 + (\alpha\rho s)_2) u)}{\partial x} + \frac{\partial(\rho\, Y_1 Y_2 u_R\, (s_1 - s_2))}{\partial x} \\ &= \Gamma\, \lambda \left(\frac{\alpha_1}{\Gamma_1 T_1} + \frac{\alpha_2}{\Gamma_2 T_2} \right) u_R^2 + \Gamma \left(\frac{1}{T_1} + \frac{1}{T_2} \right) \frac{\alpha_1}{\Gamma_1} \frac{\alpha_2}{\Gamma_2} \frac{\rho_1 C_1^2}{\alpha_1} \frac{\rho_2 C_2^2}{\alpha_2} \frac{1}{\rho C_w^2} \mathbb{A}. \end{aligned} \tag{8.37}$$

In order that the entropy inequality be fulfilled, it is sufficient to assume the term $\mathbb{A}$ to be positive or zero. Let us assume it is zero. The corresponding volume fraction equation reads

$$\begin{aligned} \frac{\mathrm{d}\alpha_1}{\mathrm{d}t} = \rho C_W^2 \frac{\alpha_1 \alpha_2}{\rho_1 C_1^2\, \rho_2 C_2^2} \Bigg[&\left((\rho_2 c_2^2 - \beta_2) - (\rho_1 c_1^2 - \beta_1) \right) \frac{\partial u}{\partial x} \\ &- \left(\frac{\rho_1 c_1^2 - \beta_1}{(\alpha\rho)_1} + \frac{\rho_2 c_2^2 - \beta_2}{(\alpha\rho)_2} \right) \frac{\partial(\rho\, Y_1 Y_2 u_R)}{\partial x} - \rho\, Y_1 Y_2 u_R \left(\frac{\Gamma_1}{\alpha_1} T_1 \frac{\partial s_1}{\partial x} + \frac{\Gamma_2}{\alpha_2} T_2 \frac{\partial s_2}{\partial x} \right) \Bigg]. \end{aligned} \tag{8.38}$$

Let us compare the right-hand side of this last equation with the equation presented in Saurel *et al.* (2008), where granular effects are absent but in the presence of

(i) mass transfer, denoted by $\dot{m}_1$, ($\dot{m}_2 = -\dot{m}_1$);

(ii) heat transfers, between the interface at temperature T_I and the phases. Those terms are denoted by $\mathbb{H}_k (T_I - T_k)$, for $k = 1,\ 2$, where the $\mathbb{H}_k$'s stand for the global heat exchange coefficients.

The corresponding volume fraction equation reads

$$\begin{aligned} \frac{\mathrm{d}\alpha_1}{\mathrm{d}t} &= \alpha_1\, \alpha_2\, \rho\, c_W^2 \left(\frac{1}{\rho_1 c_1^2} - \frac{1}{\rho_2 c_2^2} \right) \frac{\partial u}{\partial x} \\ &\quad + \rho\, c_W^2 \frac{\alpha_1 \alpha_2}{\rho_1 c_1^2\, \rho_2 c_2^2} \left(\frac{\Gamma_1}{\alpha_1} \mathbb{H}_1 (T_I - T_1) - \frac{\Gamma_2}{\alpha_2} \mathbb{H}_2 (T_I - T_2) \right) \\ &\quad + \rho\, c_W^2 \frac{1}{\rho_1 \rho_2} \left(\frac{\alpha_1}{c_1^2} + \frac{\alpha_2}{c_2^2} \right) \dot{m}_1. \end{aligned} \tag{8.39}$$

https://doi.org/10.1017/S0022112010003794 Published online by Cambridge University Press

Two terms need interpretation in the right-hand side of (8.38)

$$(a)\ \rho C_W^2 \frac{\alpha_1\alpha_2}{\rho_1 C_1^2\,\rho_2 C_2^2}\left(\frac{\rho_1 c_1^2-\beta_1}{(\alpha\rho)_1}+\frac{\rho_2 c_2^2-\beta_2}{(\alpha\rho)_2}\right)\frac{\partial(\rho\, Y_1Y_2\,u_R)}{\partial x},$$

$$(b)\ \rho C_W^2 \frac{\alpha_1\alpha_2}{\rho_1 C_1^2\,\rho_2 C_2^2}\left(\frac{\Gamma_1}{\alpha_1}\,\rho\, Y_1Y_2u_RT_1\,\frac{\partial s_1}{\partial x}+\frac{\Gamma_2}{\alpha_2}\,\rho\, Y_1Y_2u_RT_2\,\frac{\partial s_2}{\partial x}\right).$$

The first term (a) is similar to the third term in the right-hand side of (8.39)

$$\rho\, c_W^2\,\frac{1}{\rho_1\rho_2}\left(\frac{\alpha_1}{c_1^2}+\frac{\alpha_2}{c_2^2}\right)\dot{m}_1. \tag{8.40}$$

This term represents the rate of volume fraction change in the presence of mass transfer. In the present model, the mass transfer appears in differential form

$$\frac{\partial(\rho\, Y_1Y_2u_R)}{\partial x}, \tag{8.41}$$

but the meaning of the multiplying factor is the same as in (8.39). It represents the inverse of an interfacial density. As detailed in Saurel *et al.* (2008) in the context of phase transition modelling, the *mechanical relaxation* process that occurs during mass transfer is isentropic. Indeed, mass transfer produces pressure fluctuations in the phases that provoke acoustic wave propagation, responsible for pressure equilibration. These acoustic waves being isentropic, the corresponding volume fraction change is an isentropic process.

The second term (b) is the analogue of the second term of the right-hand side of (8.39)

$$\rho\, c_W^2\,\frac{\alpha_1\alpha_2}{\rho_1 c_1^2\,\rho_2 c_2^2}\left(\frac{\Gamma_1}{\alpha_1}\,\mathbb{H}_1(T_I-T_1)-\frac{\Gamma_2}{\alpha_2}\,\mathbb{H}_2(T_I-T_2)\right). \tag{8.42}$$

In the present context, the fluids are assumed inviscid and non-heat conductive. Thus, conventional heat exchanges are absent. But, generalized heat fluxes are present:

$$\rho\, Y_1Y_2u_RT_1\,\frac{\partial s_1}{\partial x}\quad\text{and}\quad\rho\, Y_1Y_2u_RT_2\,\frac{\partial s_2}{\partial x}. \tag{8.43}$$

They correspond to the heat transported by the relative motion, producing phase dilatation. The mechanical relaxation process that occurs during dilatation is also achieved, as previously, by acoustic wave propagation. Therefore, it is isentropic too.

The assumption of vanishing coefficient '$\mathbb{A}$' in the mixture entropy equation is thus justified on the basis of the acoustic processes that occur during pressure relaxation accompanied by mass transfer and generalized heat fluxes, due to inter-penetration phenomena.

The entropy equations become

$$\left.\begin{aligned}\frac{\partial(\alpha\rho s)_1}{\partial t}+\frac{\partial((\alpha\rho s)_1\,u)}{\partial x}+\frac{\partial(\rho\, Y_1Y_2u_Rs_1)}{\partial x}&=\frac{1}{T_1}\,\frac{\alpha_1}{\Gamma_1}\,\Gamma\,\lambda\,u_R^2,\\ \frac{\partial(\alpha\rho s)_2}{\partial t}+\frac{\partial((\alpha\rho s)_2\,u)}{\partial x}-\frac{\partial(\rho\, Y_1Y_2u_Rs_2)}{\partial x}&=\frac{1}{T_2}\,\frac{\alpha_2}{\Gamma_2}\,\Gamma\,\lambda\,u_R^2.\end{aligned}\right\} \tag{8.44}$$

The mixture entropy obviously agrees with the second law of thermodynamics:

$$\frac{\partial((\alpha\rho s)_1+(\alpha\rho s)_2)}{\partial t}+\frac{\partial(((\alpha\rho s)_1+(\alpha\rho s)_2)\,u)}{\partial x}+\frac{\partial(\rho\, Y_1Y_2u_R\,(s_1-s_2))}{\partial x}$$
$$=\left(\frac{1}{T_1}\,\frac{\alpha_1}{\Gamma_1}+\frac{1}{T_2}\,\frac{\alpha_2}{\Gamma_2}\right)\Gamma\,\lambda\,u_R^2\ \geqslant 0. \tag{8.45}$$

https://doi.org/10.1017/S0022112010003794 Published online by Cambridge University Press

8.5. *Summary: pressure equilibrium model with drift effects*

We summarize hereafter the thermodynamically consistent pressure equilibrium model with drift effects

$$\left.\begin{aligned}
&\frac{\mathrm{d}\alpha_1}{\mathrm{d}t} = \rho C_W^2 \frac{\alpha_1\alpha_2}{\rho_1 C_1^2\, \rho_2 C_2^2}\left[\left((\rho_2 c_2^2 - \beta_2) - (\rho_1 c_1^2 - \beta_1)\right)\frac{\partial u}{\partial x}\right.\\
&\qquad - \left(\frac{\rho_1 c_1^2 - \beta_1}{(\alpha\rho)_1} + \frac{\rho_2 c_2^2 - \beta_2}{(\alpha\rho)_2}\right)\frac{\partial(\rho\, Y_1 Y_2 u_R)}{\partial x}\\
&\qquad \left. - \rho\, Y_1 Y_2 u_R\left(\frac{\Gamma_1}{\alpha_1}\, T_1\, \frac{\partial s_1}{\partial x} + \frac{\Gamma_2}{\alpha_2}\, T_2\, \frac{\partial s_2}{\partial x}\right)\right],\\
&\frac{\partial(\alpha\rho)_1}{\partial t} + \frac{\partial((\alpha\rho)_1\, u)}{\partial x} + \frac{\partial(\rho\, Y_1 Y_2 u_R)}{\partial x} = 0,\\
&\frac{\partial(\alpha\rho)_2}{\partial t} + \frac{\partial((\alpha\rho)_2\, u)}{\partial x} - \frac{\partial(\rho\, Y_1 Y_2 u_R)}{\partial x} = 0,\\
&\frac{\partial(\rho u)}{\partial t} + \frac{\partial(\rho u^2 + P)}{\partial x} = 0,\\
&\frac{\partial(\rho E)}{\partial t} + \frac{\partial((\rho E + P)\, u)}{\partial x} + \frac{\partial(\rho\, Y_1 Y_2 u_R\,((h+B)_1 - (h+B)_2))}{\partial x} = 0,
\end{aligned}\right\} \tag{8.46}$$

where

$$\left.\begin{aligned}
&u_R = \frac{1}{\lambda}\left((\alpha_1 - Y_1)\frac{\partial P}{\partial x} - \alpha_2\frac{\partial(\alpha\beta)_1}{\partial x} + \alpha_1\frac{\partial(\alpha\beta)_2}{\partial x}\right),\\
&E = Y_1(e_1 + B_1) + Y_2(e_2 + B_2) + \frac{1}{2}u^2,\\
&P = \alpha_1 P_1 + \alpha_2 P_2.
\end{aligned}\right\} \tag{8.47}$$

The expression of the mixture pressure can easily be found in the case of stiffened gas EOS and is given by (2.44).

System (8.46)–(8.47) thus corresponds to the extension of the mechanical equilibrium model (2.33) in the limit of low velocity drift. It can be considered as an extension of the Kapila *et al.* (2001) model or as a reduction of the Baer & Nunziato (1986) model. Compared to this last one, the model is free of interfacial variables (u_I and π_I) and free of pressure relaxation parameter μ. However, the new model is restricted to low velocity drift, around the mechanical equilibrium state.

The numerical method to solve this system is described in Appendix C and is used in the following section for its validation.

9. Drift effect validation

To validate the flow model (8.46)–(8.47), a basic experimental situation is considered where gas permeation through a dense granular bed plays a major role, in the presence of pressure waves.

Let us consider a vertical shock tube filled with air ($\gamma_g = 1.4$). The experimental configuration is shown in figure 16. In the high-pressure chamber the initial air pressure and density are respectively set to

$$P_g = 3.46\,\mathrm{bar}, \quad \rho_g = 3.75\,\mathrm{kg\,m^{-3}}. \tag{9.1}$$

https://doi.org/10.1017/S0022112010003794 Published online by Cambridge University Press

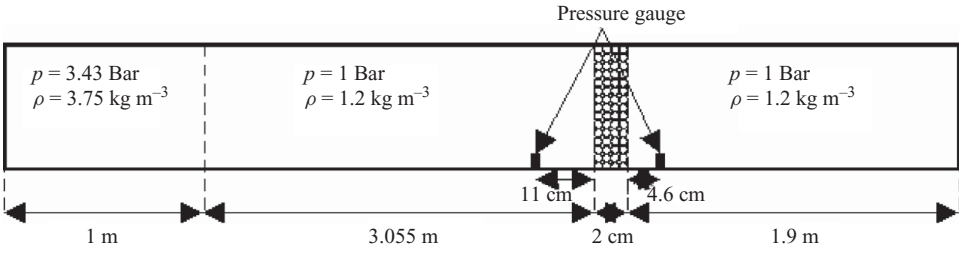


FIGURE 16. Schematic representation of the experimental shock-induced particle fluidization facility (Rogue *et al.* 1998).

The other chamber is filled with air at atmospheric pressure and density $\rho_g = 1.2\,\mathrm{kg\,m^{-3}}$. A membrane separates the two chambers. In the low-pressure chamber, a bed of small nylon solid particles is settled. Nylon particle density and volume fraction are set to

$$\rho_s = 1050\,\mathrm{kg\,m^{-3}}, \quad \alpha_s = 0.65. \tag{9.2}$$

Stiffened gas parameters for nylon are

$$\gamma_s = 4, \quad P_{s,\infty} = 600\,\mathrm{MPa}. \tag{9.3}$$

The granular EOS parameters are set to

$$a = 156\,\mathrm{kPa}, \quad n = 1.02, \quad \alpha_{s0} = 0.65. \tag{9.4}$$

At initial time, the membrane is ruptured and a shock wave propagates in the low-pressure chamber with Mach number 1.3. Then, the shock interacts with the granular bed interface and a diffraction process appears. A weak shock is transmitted through the bed while another shock is reflected. During the transmitted wave propagation, drag effects and pressure forces set the particle bed to motion. Gas permeation through the bed and drag effects produce shock weakening.

In order to examine gas permeation effects, two pressure gauges are settled. The first one is settled at a distance of 11 cm before the particle bed and the other one at a distance of 4.3 cm after. The bed thickness is 2 cm. Corresponding experiments are reported in Rogue (1997) and Rogue *et al.* (1998).

The particles are modelled as compressible, with the preceding EOS parameters. No irreversible compaction effect is considered here.

The drag force is modelled with a simple formulation as

$$\lambda = \frac{\lambda_0}{\varepsilon}, \quad \lambda_0 = \frac{1}{2}\frac{Z_1 Z_2}{Z_1 + Z_2}, \tag{9.5}$$

where λ_0 is the acoustic drag coefficient (Saurel *et al.* 2003), and ε a small positive parameter proportional to the inverse specific interfacial area ($\varepsilon \approx 1/A_I$). As for spherical particle beds of radius R_p the interfacial area reads

$$A_I = \frac{3\,\alpha_s}{R_p}, \tag{9.6}$$

we use for parameter ε an expression of the form

$$\varepsilon = \frac{\varepsilon_0}{\alpha_s}. \tag{9.7}$$

https://doi.org/10.1017/S0022112010003794 Published online by Cambridge University Press

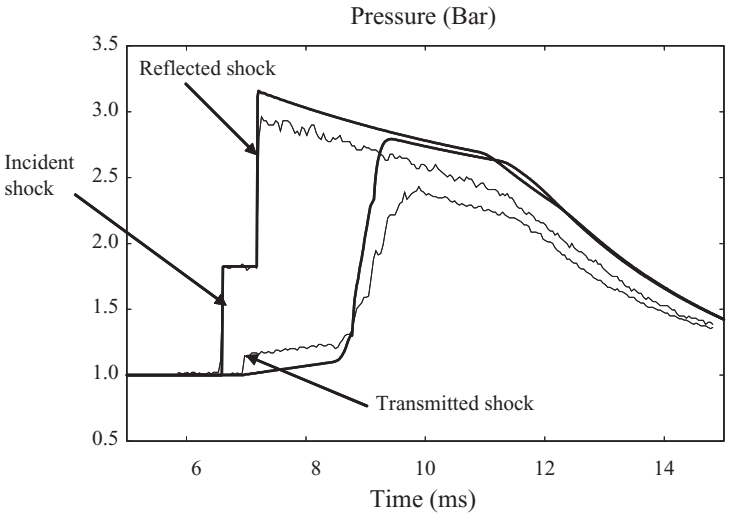


FIGURE 17. Comparison of recorded pressure signals (thin lines) with numerical computations with the flow model (8.46) in the absence of velocity drift effects (thick lines). The reflected shock is too strong and the transmitted one is too weak.

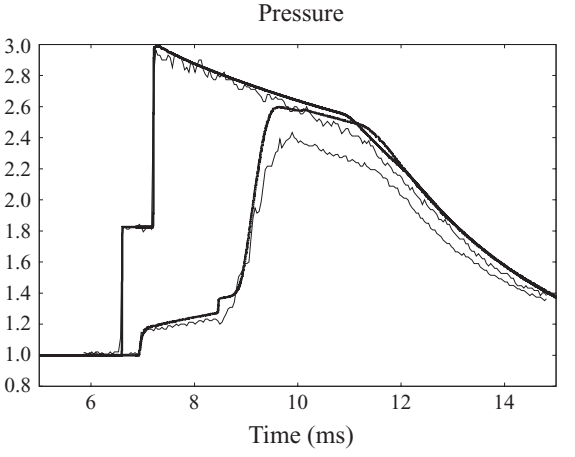


FIGURE 18. Comparison of recorded pressure signals (thin lines) versus numerical computations with the flow model (8.14) in the presence of velocity drift effects (thick lines). The reflected and transmitted shocks are of correct amplitude.

The following computations are done with

$$\varepsilon_0 = 1.23\,10^{-2}\,\mathrm{m}. \tag{9.8}$$

In figure 17, the pressure evolution on the two gauges for the case when velocity drift is absent is compared to experimental records. The experimental records are shown with thin lines and the numerical solution is shown with thick lines. Many differences are visible. When drift is absent, the transmitted shock is too weak while the reflected one is too strong.

In figure 18, the same comparison is done in the presence of drift effects. Computed results are shown with thick lines and experimental ones with thin lines.

https://doi.org/10.1017/S0022112010003794 Published online by Cambridge University Press

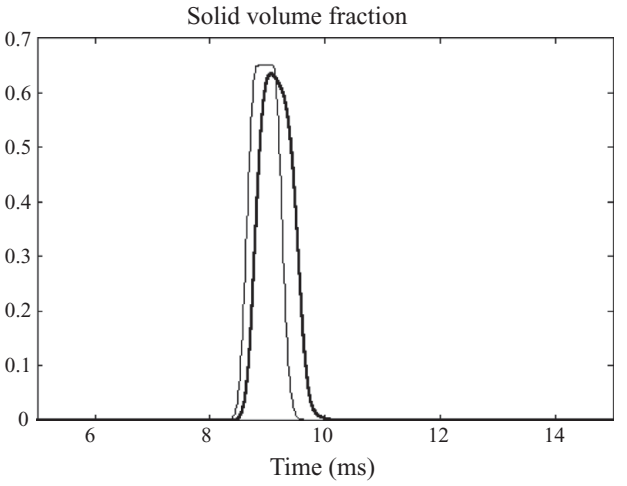


FIGURE 19. Evolution of the volume fraction at the second gauge location. The solution in the presence of drift is represented with thick lines and the solution without drift is represented with thin lines. Drift effects increase the particles bed motion and produce more diffused interfaces.

The reflected and transmitted waves are of correct amplitude. It is really at time $t = 9$ ms that some differences appear. The level of the computed pressure on the second gauge is higher than the experimental one. Those differences appear after the particle bed has passed the second pressure gauge location. In figure 19, time evolution of the volume fraction in the presence of drift effects is shown. When the particles bed has passed the second gauge (after 10 ms) we should get the same pressure level for the two gauges while they appear to be different on the experimental records. We suspect that pressure gauges present some deviations.

10. Conclusion

A multiphase flow model for the irreversible compaction of powders has been built and validated. It is free of adjustable parameters and is able to reproduce with fidelity loading–unloading cycles as well as interface dynamics separating fluids and granular mixtures. Its numerical resolution has been achieved on the basis of simple extension of the method given in Saurel *et al.* (2009). Moreover, the model perfectly fits the frame of diffuse interface theory, used for different types of flow problems, ranging from material interfaces, cavitating flows (Saurel *et al.* 2008), capillary fluids (Périgaud & Saurel 2005), and solid–fluid interfaces (Favrie, Gavrilyuk & Saurel 2009). Very different type of physics can be inserted in this frame.

Another extension is done regarding gas permeation effects, resulting in a velocity non-equilibrium model, where the only adjustable parameters are related to conventional drag force correlations. The corresponding model can also be considered as a diffuse interface model with inter-penetration effects.

This work was partially supported by DGA – CEA Centre d'Etudes de gramat. The authors are particularly grateful to E. Lapebie and G. Baudin. They also address special thanks to the referees for important remarks that helped manuscript improvements.

https://doi.org/10.1017/S0022112010003794 Published online by Cambridge University Press

Appendix A. Asymptotic limit of the pressure non-equilibrium model with stiff mechanical relaxation

Let us assume that the pressure relaxation coefficient is of the form $\mu = \mu_0/\varepsilon$, with $\varepsilon \to 0^+$. Each flow variable f is assumed to obey an asymptotic expansion of the form: $f = f^0 + \varepsilon f^1$, where f^0 represents the equilibrium state and f^1 represents a small perturbation around it.

With these notations, the volume fraction equation of the non-equilibrium system (3.1),

$$\frac{\partial \alpha_1}{\partial t} + u\frac{\partial \alpha_1}{\partial x} = \mu(\pi_1 - \pi_2), \tag{A 1}$$

becomes

$$\frac{\mathrm{d}\alpha_1^0}{\mathrm{d}t} = \frac{\mu_0}{\varepsilon}\left(\pi_1^0 - \pi_2^0\right) + \mu_0\left(\pi_1^1 - \pi_2^1\right). \tag{A 2}$$

This equation implies two new equations. The first one expresses evolutions at zero-order

$$\frac{\mathrm{d}\alpha_1^0}{\mathrm{d}t} = \mu_0\left(\pi_1^1 - \pi_2^1\right), \tag{A 3}$$

the second one expresses evolutions at $1/\varepsilon$ order:

$$\frac{\mu_0}{\varepsilon}\left(\pi_1^0 - \pi_2^0\right) = 0. \tag{A 4}$$

The mechanical equilibrium condition is thus recovered:

$$\pi_1^0 = \pi_2^0 = \pi^0. \tag{A 5}$$

Determining the pressure fluctuation difference $(\pi_1^1 - \pi_2^1)$ needs evolution equation for the pressures π_k. From the internal energy equations of (3.1), there is no difficulty to determine the thermodynamic pressure equations. Here an example is given for phase 1:

$$\frac{\mathrm{d}P_1}{\mathrm{d}t} + \rho_1 c_1^2 \frac{\partial u}{\partial x} = -\frac{\Gamma_1}{\alpha_1}\left(\pi_I - \pi_1 + \frac{\rho_1 c_1^2}{\Gamma_1}\right)\mu(\pi_1 - \pi_2). \tag{A 6}$$

It is then necessary to determine the evolution equation for the granular pressure. To this end, (2.22) is used:

$$\beta_1 = (\alpha\rho)_1 \frac{\mathrm{d}B_1}{\mathrm{d}\alpha_1}. \tag{A 7}$$

Differentiation along a trajectory gives

$$\frac{\mathrm{d}\beta_1}{\mathrm{d}t} = -\beta_1 \frac{\partial u}{\partial x} + (\alpha\rho)_1 \frac{\mathrm{d}^2 B_1}{\mathrm{d}{\alpha_1}^2}\mu(\pi_1 - \pi_2). \tag{A 8}$$

Taking the difference of (A 6) and (A 8) we obtain

$$\frac{\mathrm{d}(P_1 - \beta_1)}{\mathrm{d}t} + \left(\rho_1 c_1^2 - \beta_1\right)\frac{\partial u}{\partial x} = -\frac{\Gamma_1}{\alpha_1}\left(\pi_I - \pi_1 + \frac{\rho_1}{\Gamma_1}\left(c_1^2 + \alpha_1^2 \frac{\mathrm{d}^2 B_1}{\mathrm{d}{\alpha_1}^2}\right)\right)\mu(\pi_1 - \pi_2). \tag{A 9}$$

Denoting

$$C_1^2 = c_1^2 + \alpha_1^2 \frac{\mathrm{d}^2 B_1}{\mathrm{d}{\alpha_1}^2}, \tag{A 10}$$

https://doi.org/10.1017/S0022112010003794 Published online by Cambridge University Press

the pressure evolution equation becomes

$$\frac{\mathrm{d}\pi_1}{\mathrm{d}t} + \left(\rho_1 c_1^2 - \beta_1\right)\frac{\partial u}{\partial x} = -\frac{\Gamma_1}{\alpha_1}\left(\pi_I - \pi_1 + \frac{\rho_1 C_1^2}{\Gamma_1}\right)\mu(\pi_1 - \pi_2). \tag{A 11}$$

We now introduce in this equation equilibrium variables and their fluctuations. It becomes

$$\frac{\mathrm{d}\pi_1^0}{\mathrm{d}t} + \left(\rho_1^0 \left(c_1^0\right)^2 - \beta_1^0\right)\frac{\partial u^0}{\partial x} = -\frac{\Gamma_1^0}{\alpha_1^0}\left(\pi_I^0 - \pi_1^0 + \frac{\rho_1^0 \left(C_1^2\right)^0}{\Gamma_1^0}\right)\mu_0\left(\pi_1^1 - \pi_2^1\right). \tag{A 12}$$

Using (A 5) we have

$$\frac{\mathrm{d}\pi_1^0}{\mathrm{d}t} + \left(\rho_1^0 \left(c_1^0\right)^2 - \beta_1^0\right)\frac{\partial u^0}{\partial x} = -\frac{\rho_1^0 \left(C_1^2\right)^0}{\alpha_1^0}\mu_0\left(\pi_1^1 - \pi_2^1\right). \tag{A 13}$$

For the other phase, similarly we have

$$\frac{\mathrm{d}\pi_2^0}{\mathrm{d}t} + \left(\rho_2^0 \left(c_2^0\right)^2 - \beta_2^0\right)\frac{\partial u^0}{\partial x} = \frac{\rho_2^0 \left(C_2^2\right)^0}{\alpha_2^0}\mu_0\left(\pi_1^1 - \pi_2^1\right). \tag{A 14}$$

Taking the difference of these two equations, we finally obtain

$$\mu_0\left(\pi_1^1 - \pi_2^1\right) = \frac{\left(\rho_2^0 \left(c_2^0\right)^2 - \beta_2^0\right) - \left(\rho_1^0 \left(c_1^0\right)^2 - \beta_1^0\right)}{\dfrac{\rho_1^0 \left(C_1^2\right)^0}{\alpha_1^0} + \dfrac{\rho_2^0 \left(C_2^2\right)^0}{\alpha_2^0}}\frac{\partial u^0}{\partial x}. \tag{A 15}$$

The volume fraction equation is thus

$$\frac{\mathrm{d}\alpha_1^0}{\mathrm{d}t} = \frac{\left(\rho_2^0 \left(c_2^0\right)^2 - \beta_2^0\right) - \left(\rho_1^0 \left(c_1^0\right)^2 - \beta_1^0\right)}{\dfrac{\rho_1^0 \left(C_1^2\right)^0}{\alpha_1^0} + \dfrac{\rho_2^0 \left(C_2^2\right)^0}{\alpha_2^0}}\frac{\partial u^0}{\partial x}. \tag{A 16}$$

This equation is in perfect agreement with the first equation of system (2.33).

Appendix B. Frozen and equilibrium sound speed inequalities

Consider the equilibrium of a granular solid with a gas. The mechanical equilibrium condition and the mixture pressure definitions are, respectively,

$$\left.\begin{aligned} &\pi_1 = P_1 - Y_1\,\rho\,\frac{\mathrm{d}B_1}{\mathrm{d}\alpha_1}(\alpha_1) = \pi_2 = P_2, \\ &P = \rho^2\frac{\partial e}{\partial \rho} = \alpha_1 P_1 + \alpha_2 P_2. \end{aligned}\right\} \tag{B 1}$$

We need to obtain the expression for the equilibrium sound speed. Differentiating the equilibrium condition gives

$$c_1^2\left(-\frac{Y_1\,\rho}{\alpha_1^2}\frac{\mathrm{d}\alpha_1}{\mathrm{d}t} + \frac{Y_1}{\alpha_1}\frac{\mathrm{d}\rho}{\mathrm{d}t}\right) - Y_1\left(\frac{\mathrm{d}\rho}{\mathrm{d}t}\frac{\mathrm{d}B_1}{\mathrm{d}\alpha_1}(\alpha_1) + \rho\frac{\mathrm{d}^2 B_1}{\mathrm{d}{\alpha_1}^2}(\alpha_1)\frac{\mathrm{d}\alpha_1}{\mathrm{d}t}\right) = c_2^2\left(-\frac{Y_2\,\rho}{\alpha_2^2}\frac{\mathrm{d}\alpha_2}{\mathrm{d}t} + \frac{Y_2}{\alpha_2}\frac{\mathrm{d}\rho}{\mathrm{d}t}\right) \tag{B 2}$$

https://doi.org/10.1017/S0022112010003794 Published online by Cambridge University Press

or

$$\left(\frac{Y_1\,c_1^2}{\alpha_1}-\frac{Y_2\,c_2^2}{\alpha_2}-Y_1\,\frac{\mathrm{d}B_1}{\mathrm{d}\alpha_1}(\alpha_1)\right)\frac{\mathrm{d}\rho}{\mathrm{d}t}=\left(\frac{Y_1\,\rho\,c_1^2}{\alpha_1^2}+\frac{Y_2\,\rho\,c_2^2}{\alpha_2^2}+Y_1\,\rho\,\frac{\mathrm{d}^2B_1}{\mathrm{d}{\alpha_1}^2}(\alpha_1)\right)\frac{\mathrm{d}\alpha_1}{\mathrm{d}t}. \quad (B\,3)$$

Differentiating the pressure definition, we get

$$\begin{aligned}\frac{\mathrm{d}P}{\mathrm{d}t}&=\frac{\mathrm{d}\alpha_1}{\mathrm{d}t}(P_1-P_2)+\alpha_1\,c_1^2\left(-\frac{Y_1\,\rho}{\alpha_1^2}\frac{\mathrm{d}\alpha_1}{\mathrm{d}t}+\frac{Y_1}{\alpha_1}\frac{\mathrm{d}\rho}{\mathrm{d}t}\right)+\alpha_2\,c_2^2\left(-\frac{Y_2\,\rho}{\alpha_2^2}\frac{\mathrm{d}\alpha_2}{\mathrm{d}t}+\frac{Y_2}{\alpha_2}\frac{\mathrm{d}\rho}{\mathrm{d}t}\right)\\&=\frac{\mathrm{d}\alpha_1}{\mathrm{d}t}\left(P_1-P_2-\frac{Y_1\,\rho\,c_1^2}{\alpha_1}+\frac{Y_2\,\rho\,c_2^2}{\alpha_2}\right)+\frac{\mathrm{d}\rho}{\mathrm{d}t}\left(Y_1\,c_1^2+Y_2\,c_2^2\right). \quad (B\,4)\end{aligned}$$

Combining (B 3) and (B 4) we get

$$\frac{\mathrm{d}P}{\mathrm{d}t}=\frac{\mathrm{d}\rho}{\mathrm{d}t}\left(Y_1c_1^2+Y_2c_2^2-\frac{\left(\left(\frac{Y_1\,c_1^2}{\alpha_1}-Y_1\,\frac{\mathrm{d}B_1}{\mathrm{d}\alpha_1}(\alpha_1)\right)-\frac{Y_2\,c_2^2}{\alpha_2}\right)^2}{\frac{Y_1\,c_1^2}{\alpha_1^2}+\frac{Y_2\,c_2^2}{\alpha_2^2}+Y_1\,\frac{\mathrm{d}^2B_1}{\mathrm{d}{\alpha_1}^2}(\alpha_1)}\right). \quad (B\,5)$$

Let us define the equilibrium sound speed by

$$c_W^2=c_f^2-\frac{\left(\left(\frac{Y_1\,c_1^2}{\alpha_1}-Y_1\,\frac{\mathrm{d}B_1}{\mathrm{d}\alpha_1}(\alpha_1)\right)-\frac{Y_2\,c_2^2}{\alpha_2}\right)^2}{\frac{Y_1\,c_1^2}{\alpha_1^2}+\frac{Y_2\,c_2^2}{\alpha_2^2}+Y_1\,\frac{\mathrm{d}^2B_1}{\mathrm{d}{\alpha_1}^2}(\alpha_1)}, \quad (B\,6)$$

here, $c_f^2=Y_1\,c_1^2+Y_2\,c_2^2$ represents the frozen sound speed. Obviously, $c_f^2>c_W^2$.

Let us remark that the conventional equilibrium sound speed (when $B_1(\alpha_1)=0$) is

$$c_{W,fluids}^2=\frac{\frac{Y_1\,c_1^2}{\alpha_1^2}\,\frac{Y_2\,c_2^2}{\alpha_2^2}}{\frac{Y_1\,c_1^2}{\alpha_1^2}+\frac{Y_2\,c_2^2}{\alpha_2^2}} \quad (B\,7)$$

or

$$\frac{1}{c_{W,fluids}^2}=\frac{\alpha_1^2}{Y_1\,c_1^2}+\frac{\alpha_2^2}{Y_2\,c_2^2}. \quad (B\,8)$$

The difference between the Wood sound speed with granular effects and the conventional one for fluid mixtures is therefore

$$c_W^2-c_{W,fluids}^2=\frac{1}{\rho}\left(\frac{\left(\rho_2\,c_2^2-\rho_1\,c_1^2\right)^2}{\frac{\rho_1\,c_1^2}{\alpha_1}+\frac{\rho_2\,c_2^2}{\alpha_2}}-\frac{\left(\rho_1\left(c_1^2-\alpha_1\,\frac{\mathrm{d}B_1}{\mathrm{d}\alpha_1}(\alpha_1)\right)-\rho_2\,c_2^2\right)^2}{\frac{\rho_1\,c_1^2}{\alpha_1}+\frac{\rho_2\,c_2^2}{\alpha_2}+\alpha_1\,\rho_1\,\frac{\mathrm{d}^2B_1}{\mathrm{d}{\alpha_1}^2}(\alpha_1)}\right). \quad (B\,9)$$

We will suppose that

$$\rho_1c_1^2-\rho_2c_2^2>0,\quad \rho_1c_1^2-\rho_2\,c_2^2-(\alpha\rho)_1\,\frac{\mathrm{d}B_1}{\mathrm{d}\alpha_1}(\alpha_1)>0 \quad (B\,10)$$

and

$$\frac{\mathrm{d}B_1}{\mathrm{d}\alpha_1}(\alpha_1)>0,\quad \frac{\mathrm{d}^2B_1}{\mathrm{d}{\alpha_1}^2}(\alpha_1)>0. \quad (B\,11)$$

https://doi.org/10.1017/S0022112010003794 Published online by Cambridge University Press

The inequalities (B 10) are usually valid as the solid sound speed is dominant compared to the gas sound speed and the *configuration* sound speed. Inequalities (B 11) are also verified with our expression of $B_1(\alpha_1)$. Consequently,

$$c_W^2 - c_{W,fluids}^2 > 0. \tag{B 12}$$

The *granular* Wood sound speed is always larger than the conventional one, if (B 10) is valid and if $B_1(\alpha_1)$ is a monotically increasing and convex function.

Appendix C. Numerical method to solve the drift model

The system to solve corresponds to system (8.46)–(8.47). This system is split in a hyperbolic subsystem and a *diffusive* one, solved separately.

C.1. *Hyperbolic step*

The aim is to solve the following system:

$$\left.\begin{aligned}
&\frac{\mathrm{d}\alpha_1}{\mathrm{d}t} = \rho C_W^2 \frac{\alpha_1\alpha_2}{\rho_1 C_1^2 \rho_2 C_2^2}\left(\left(\rho_2 c_2^2 - \beta_2\right) - \left(\rho_1 c_1^2 - \beta_1\right)\right)\frac{\partial u}{\partial x},\\
&\frac{\partial(\alpha\rho)_1}{\partial t} + \frac{\partial((\alpha\rho)_1 u)}{\partial x} = 0,\\
&\frac{\partial(\alpha\rho)_2}{\partial t} + \frac{\partial((\alpha\rho)_2 u)}{\partial x} = 0,\\
&\frac{\partial(\rho u)}{\partial t} + \frac{\partial(\rho u^2 + P)}{\partial x} = 0,\\
&\frac{\partial(\rho E)}{\partial t} + \frac{\partial((\rho E + P) u)}{\partial x} = 0,
\end{aligned}\right\} \tag{C 1}$$

with

$$E = Y_1 (e_1 + B_1) + Y_2(e_2 + B_2) + \tfrac{1}{2}u^2, \quad P = \alpha_1 P_1 + \alpha_2 P_2. \tag{C 2}$$

This system corresponds to the one already considered in § 5.

C.2. *Drift step*

In this step, we have to solve

$$\left.\begin{aligned}
&\frac{\partial\alpha_1}{\partial t} = -\rho C_W^2 \frac{\alpha_1\alpha_2}{\rho_1 C_1^2 \rho_2 C_2^2}\,\mathbb{A}_D,\\
&\frac{\partial(\alpha\rho)_1}{\partial t} + \frac{\partial(\rho Y_1 Y_2 u_R)}{\partial x} = 0,\\
&\frac{\partial(\alpha\rho)_2}{\partial t} - \frac{\partial(\rho Y_1 Y_2 u_R)}{\partial x} = 0,\\
&\frac{\partial(\rho u)}{\partial t} = 0,\\
&\frac{\partial(\rho E)}{\partial t} + \frac{\partial(\rho\, Y_1 Y_2 u_R((h+B)_1 - (h+B)_2))}{\partial x} = 0,
\end{aligned}\right\} \tag{C 3}$$

https://doi.org/10.1017/S0022112010003794 Published online by Cambridge University Press

with

$$\left.\begin{aligned} u_R &= \frac{1}{\lambda}\left((\alpha_1 - Y_1)\frac{\partial P}{\partial x} - \alpha_2\frac{\partial(\alpha\beta)_1}{\partial x} + \alpha_1\frac{\partial(\alpha\beta)_2}{\partial x}\right),\\ E &= Y_1(e_1 + B_1) + Y_2(e_2 + B_2) + \frac{1}{2}u^2,\\ P &= \alpha_1 P_1 + \alpha_2 P_2,\\ \mathbb{A}_D &= \left(\frac{\rho_1 c_1^2 - \beta_1}{\alpha_1\rho_1} + \frac{\rho_2 c_2^2 - \beta_2}{\alpha_2\rho_2}\right)\frac{\partial(\rho Y_1 Y_2 u_R)}{\partial x} + \rho\, Y_1 Y_2 u_R\left(\frac{\Gamma_1}{\alpha_1}T_1\frac{\partial s_1}{\partial x} + \frac{\Gamma_2}{\alpha_2}T_2\frac{\partial s_2}{\partial x}\right). \end{aligned}\right\} \tag{C 4}$$

Two internal energy equations, which are consequences of (C 3), can be considered too

$$\left.\begin{aligned} \frac{\partial(\alpha\rho e)_1}{\partial t} + \frac{\partial(\rho\, Y_1 Y_2 u_R\, e_1)}{\partial x} + P_1\frac{\partial}{\partial x}\left(\frac{\rho\, Y_1 Y_2 u_R}{\rho_1}\right) &= -P_1\frac{\partial\alpha_1}{\partial t} + \frac{\alpha_1}{\Gamma_1}\Gamma\lambda u_R^2,\\ \frac{\partial(\alpha\rho e)_2}{\partial t} - \frac{\partial(\rho\, Y_1 Y_2 u_R\, e_2)}{\partial x} - P_2\frac{\partial}{\partial x}\left(\frac{\rho\, Y_1 Y_2 u_R}{\rho_2}\right) &= +P_2\frac{\partial\alpha_1}{\partial t} + \frac{\alpha_2}{\Gamma_2}\Gamma\lambda u_R^2, \end{aligned}\right\} \tag{C 5}$$

The resolution method follows the same three steps as used previously to solve system (C 1):

(*a*) Diffusion step and solution prediction: During this step the various diffusion terms are considered, but only part of the volume fraction equation is solved:

$$\frac{\partial\alpha_1}{\partial t} = -\rho C_W^2\frac{\alpha_1\alpha_2}{\rho_1 C_1^2\,\rho_2 C_2^2}\left(\frac{\rho_1 c_1^2 - \beta_1}{(\alpha\rho)_1} + \frac{\rho_2 c_2^2 - \beta_2}{(\alpha\rho)_2}\right)\frac{\partial(\rho\, Y_1 Y_2 u_R)}{\partial x}. \tag{C 6}$$

(*b*) Pressure relaxation step: Remaining volume fraction equation terms are addressed with a relaxation method.

(*c*) Reset step and solution correction: Correction is done to preserve mixture total energy.

C.2.1. *Diffusion step*

The subsystem considered during this step reads as

$$\left.\begin{aligned} &\frac{\partial\alpha_1}{\partial t} = -\rho C_W^2\,\frac{\alpha_1\alpha_2}{\rho_1 C_1^2\,\rho_2 C_2^2}\left(\frac{\rho_1 c_1^2 - \beta_1}{(\alpha\rho)_1} + \frac{\rho_2 c_2^2 - \beta_2}{(\alpha\rho)_2}\right)\frac{\partial(\rho\, Y_1 Y_2 u_R)}{\partial x},\\ &\frac{\partial(\alpha\rho e)_1}{\partial t} + \frac{\partial(\rho\, Y_1 Y_2 u_R\, e_1)}{\partial x} + P_1\frac{\partial}{\partial x}\left(\frac{\rho\, Y_1 Y_2 u_R}{\rho_1}\right) = -P_1\frac{\partial\alpha_1}{\partial t},\\ &\frac{\partial(\alpha\rho e)_2}{\partial t} - \frac{\partial(\rho\, Y_1 Y_2 u_R\, e_2)}{\partial x} - P_2\frac{\partial}{\partial x}\left(\frac{\rho\, Y_1 Y_2 u_R}{\rho_2}\right) = +P_2\frac{\partial\alpha_1}{\partial t},\\ &\frac{\partial(\alpha\rho)_1}{\partial t} + \frac{\partial(\rho\, Y_1 Y_2 u_R)}{\partial x} = 0,\\ &\frac{\partial(\alpha\rho)_2}{\partial t} - \frac{\partial(\rho\, Y_1 Y_2 u_R)}{\partial x} = 0,\\ &\frac{\partial(\rho u)}{\partial t} = 0,\\ &\frac{\partial(\rho E)}{\partial t} + \frac{\partial(\rho\, Y_1 Y_2 u_R\,((h+B)_1 - (h+B)_2))}{\partial x} = 0. \end{aligned}\right\} \tag{C 7}$$

https://doi.org/10.1017/S0022112010003794 Published online by Cambridge University Press

C.2.2. *Mass equations*

The following explicit scheme is used for the mass equations. Let us consider the mass equation for phase 1:

$$\frac{\partial(\alpha\rho)_1}{\partial t} + \frac{\partial(\rho\, Y_1 Y_2 u_R)}{\partial x} = 0. \tag{C 8}$$

The mass flux is denoted by

$$q = q_1 + q_2 + q_3, \tag{C 9}$$

where

$$\left.\begin{aligned} q_1 &= \omega_1 \frac{\partial \pi}{\partial x}, \qquad \omega_1 = \frac{1}{\lambda}\rho\, Y_1 Y_2 (\alpha_1 - Y_1), \\ q_2 &= \omega_2 \frac{\partial(\alpha\beta)_1}{\partial x}, \quad \omega_2 = \frac{1}{\lambda}\rho\, Y_1 Y_2^2, \\ q_3 &= \omega_3 \frac{\partial(\alpha\beta)_2}{\partial x}, \quad \omega_3 = \frac{1}{\lambda}\rho\, Y_1^2 Y_2. \end{aligned}\right\} \tag{C 10}$$

Space and time integration of the mass equation gives

$$(\alpha\rho)_{1,i}^{n+1} = (\alpha\rho)_{1,i}^{n} - \frac{\Delta t}{\Delta x}\left(q^*_{i+1/2} - q^*_{i-1/2}\right). \tag{C 11}$$

The mass fluxes at cell boundaries $i \pm 1/2$ have to be determined. The following conditions are used: at a given cell boundary flux conservation must be preserved:

$$q_k^{*-} = q_k^{*+} = q_k^*. \tag{C 12}$$

The diffusive character of the mass equation guarantees continuity of the constraints

$$\left.\begin{aligned} \pi^{*-} &= \pi^{*+} = \pi^*, \\ (\alpha\beta)_k^{*-} &= (\alpha\beta)_k^{*+} = (\alpha\beta)^*. \end{aligned}\right\} \tag{C 13}$$

Expressed at cell boundary $i - 1/2$, these conditions imply

$$\left.\begin{aligned} &\omega_{1,L}(\pi^* - \pi_{i-1}) = \omega_{1,R}(\pi_i - \pi^*), \\ &\omega_{2,L}((\alpha\beta)_1^* - (\alpha\beta)_{1,i-1}) = \omega_{2,R}((\alpha\beta)_{1,i} - (\alpha\beta)_1^*), \\ &\omega_{3,L}((\alpha\beta)_2^* - (\alpha\beta)_{2,i-1}) = \omega_{3,R}((\alpha\beta)_{2,i} - (\alpha\beta)_2^*). \end{aligned}\right\} \tag{C 14}$$

They determine the inter-cell parameters

$$\left.\begin{aligned} \pi^* &= \frac{\omega_{1,R}\pi_i + \omega_{1,L}\pi_{i-1}}{\omega_{1,L} + \omega_{1,R}}, \\ (\alpha\beta)_1^* &= \frac{\omega_{2,R}(\alpha\beta)_{1,i} + \omega_{2,L}(\alpha\beta)_{1,i-1}}{\omega_{2,L} + \omega_{2,R}}, \\ (\alpha\beta)_2^* &= \frac{\omega_{3,R}(\alpha\beta)_{2,i} + \omega_{3,L}(\alpha\beta)_{2,i-1}}{\omega_{3,L} + \omega_{3,R}}. \end{aligned}\right\} \tag{C 15}$$

The corresponding fluxes are then

$$\left.\begin{aligned} q^*_{1,i-1/2} &= 2\,\frac{\omega_{1,L}\,\omega_{1,R}}{\omega_{1,L} + \omega_{1,R}}\,\frac{\pi_i - \pi_{i-1}}{\Delta x}, \\ q^*_{2,i-1/2} &= 2\,\frac{\omega_{2,L}\,\omega_{2,R}}{\omega_{2,L} + \omega_{2,R}}\,\frac{(\alpha\beta)_{1,i} - (\alpha\beta)_{1,i-1}}{\Delta x}, \\ q^*_{3,i-1/2} &= 2\,\frac{\omega_{3,L}\,\omega_{3,R}}{\omega_{3,L} + \omega_{3,R}}\,\frac{(\alpha\beta)_{2,i} - (\alpha\beta)_{2,i-1}}{\Delta x}. \end{aligned}\right\} \tag{C 16}$$

https://doi.org/10.1017/S0022112010003794 Published online by Cambridge University Press

These fluxes are summed up and used to update the mass equations with (C 11) and the same algorithm is used for the second phase.

C.2.3. *Energy and volume fraction equations*

Let us consider the internal energy equation for phase 1. It reads as

$$\frac{\partial(\alpha\rho e)_1}{\partial t} + \frac{\partial(\rho\, Y_1 Y_2 u_R\, e_1)}{\partial x} + P_1 \frac{\partial}{\partial x}\left(\frac{\rho\, Y_1 Y_2 u_R}{\rho_1}\right) = -P_1 \frac{\partial \alpha_1}{\partial t}. \tag{C 17}$$

With the help of the mass and volume fraction equations it becomes

$$\frac{\partial s_1}{\partial t} + \frac{\rho\, Y_1 Y_2 u_R}{(\alpha\rho)_1} \frac{\partial s_1}{\partial x} = 0. \tag{C 18}$$

It means that once the mass flux is determined at a given cell boundary, the transport velocity sign in the entropy equation is determined too. At cell boundary $(i-1/2)$, it reads as

$$s^*_{1,i-1/2} = \begin{cases} s_{1,i-1} & \text{if } q^*_{i-1/2} \geqslant 0, \\ s_{1,i} & \text{otherwise.} \end{cases} \tag{C 19}$$

Therefore, the entropies are known at cell boundaries. At a given cell boundary, variables π^*, $(\alpha\beta)^*_k$, s^*_k, for $k = 1, 2$ are now known, hence it is possible to determine the remaining variables.

Equation (C 19) is expressed as

$$\rho^*_{1,i-1/2} = \begin{cases} \rho_{1,i-1}\left(\dfrac{P^*_{1,i-1/2} + P_{1,\infty}}{P_{1,i-1} + P_{1,\infty}}\right)^{1/\gamma_1} & \text{if } q^*_{i-1/2} \geqslant 0, \\ \rho_{1,i}\left(\dfrac{P^*_{1,i-1/2} + P_{1,\infty}}{P_{1,i} + P_{1,\infty}}\right)^{1/\gamma_1} & \text{otherwise,} \end{cases} \tag{C 20}$$

$$\rho^*_{2,i-1/2} = \begin{cases} \rho_{2,i}\left(\dfrac{P^*_{2,i-1/2} + P_{2,\infty}}{P_{2,i} + P_{2,\infty}}\right)^{1/\gamma_2} & \text{if } q^*_{i-1/2} \geqslant 0, \\ \rho_{2,i-1}\left(\dfrac{P^*_{2,i-1/2} + P_{2,\infty}}{P_{2,i-1} + P_{2,\infty}}\right)^{1/\gamma_2} & \text{otherwise.} \end{cases} \tag{C 21}$$

The inter-cell pressures in these relations are computed from

$$\left.\begin{aligned} P^*_k &= \pi^* + \frac{(\alpha\beta)^*_k}{\alpha^*_k}, \\ (\alpha\beta)^*_k &= (\alpha^*_k)^2\, \rho^*_k\, \frac{\mathrm{d}B_k}{\mathrm{d}\alpha_k}(\alpha^*_k). \end{aligned}\right\} \tag{C 22}$$

Indeed, as π^*, $(\alpha\beta)^*_k$ and the pressures P^*_k become only function of the volume fraction: $P^*_k = P^*_k(\alpha^*_k)$. Inserted in (C 20), the densities become also function of the volume fractions: $\rho^*_k = \rho^*_k(\alpha^*_k)$. The volume fraction is the correct one when the second equation of system (C 22) is satisfied. The Newton–Raphson method is used to solve system (C 20)–(C 22).

From the inter-cell pressures and densities, there is no difficulty to determine the remaining thermodynamic variables $e^*_{1,i-1/2}$ and $h^*_{1,i-1/2}$. The total energy evolution is

https://doi.org/10.1017/S0022112010003794 Published online by Cambridge University Press

thus approximated by

$$(\rho E)_{,i}^{n+1} = (\rho E)_{,i}^{n} - \frac{\Delta t}{\Delta x}\left[q^*_{i+1/2}\left((h+B)^*_{1,i+1/2} - (h+B)^*_{2,i+1/2}\right) - q^*_{i-1/2}\left((h+B)^*_{1,i-1/2} - (h+B)^*_{2,i-1/2}\right)\right]. \quad (C\,23)$$

The internal energy equations contain extra terms that cannot be expressed under conservative form. Their accurate integration is thus an issue. The same type of difficulty was present with the non-conservative terms of the internal energy equations during the hyperbolic step. The simplest approximation was retained for these terms, keeping in mind that these equations were just used to predict the solution. We adopt here the same strategy with the following simple approximation:

$$\begin{aligned}(\alpha\rho e)_{1,i}^{n+1} = {} & (\alpha\rho e)_{1,i}^{n} - \frac{\Delta t}{\Delta x}\left(q^*_{i+1/2}\, h^*_{1,i+1/2} - q^*_{i-1/2}\, h^*_{1,i-1/2}\right) \\ & + \frac{\Delta t}{\Delta x}\left(\frac{\rho\, Y_1 Y_2 u_R}{\rho_1}\right)^n_i \left(P^*_{1,i+1/2} - P^*_{1,i-1/2}\right) \\ & - \frac{\Delta t}{\Delta x}\left[\frac{\rho C_W^2}{\rho_1 C_1^2\, \rho_2 C_2^2}\, P_1 \left(\frac{\beta_1 - \rho_1 c_1^2}{(\alpha\rho)_1} + \frac{\beta_2 - \rho_2 c_2^2}{(\alpha\rho)_2}\right)\right]^n_i \left(q^*_{i+1/2} - q^*_{i-1/2}\right) \\ & + \Delta t \left(\frac{\alpha_1}{\Gamma_1}\,\Gamma\,\lambda\right)^n_i (u^n_{R,i})^2 \end{aligned} \quad (C\,24)$$

with

$$u^n_{R,i} = \frac{1}{\lambda_0}\left[\left(\alpha^n_{1,i} - Y^n_{1,i}\right)\frac{\pi^*_{i+1/2} - \pi^*_{i-1/2}}{\Delta x} + Y^n_{2,i}\,\frac{\alpha^*_{1,i+1/2}\,\beta^*_{1,i+1/2} - \alpha^*_{1,i-1/2}\,\beta^*_{1,i-1/2}}{\Delta x} - Y^n_{1,i}\,\frac{\alpha^*_{2,i+1/2}\,\beta^*_{2,i+1/2} - \alpha^*_{2,i-1/2}\,\beta^*_{2,i-1/2}}{\Delta x}\right]. \quad (C\,25)$$

Similarly, the volume fraction equation is approximated as

$$\alpha^{n+1}_{1,i} = \alpha^n_{1,i} - \frac{\Delta t}{\Delta x}\left(\rho C_W^2\,\frac{\alpha_1\alpha_2}{\rho_1 C_1^2\,\rho_2 C_2^2}\left(\frac{\rho_1 c_1^2 - \beta_1}{(\alpha\rho)_1} + \frac{\rho_2 c_2^2 - \beta_2}{(\alpha\rho)_2}\right)\right)^n_i \left(q^*_{i+1/2} - q^*_{i-1/2}\right). \quad (C\,26)$$

Similar approximation formulae are used for the second phase.

This method is stable if the following stability criterion is fulfilled:

$$\Delta t \leqslant \frac{\Delta x^2}{\max_i\left[\rho C_W^2 q\left(\dfrac{\rho_2 c_2^2 - \beta_2}{\rho_2^2 C_2^2} - \dfrac{\rho_1 c_1^2 - \beta_1}{\rho_1^2 C_1^2}\right)\right]_i}. \quad (C\,27)$$

This criterion is deduced from the pressure evolution equation:

$$\begin{aligned} & \frac{\mathrm{d}\pi}{\mathrm{d}t} + \rho C_W^2 \left[\left(\frac{\alpha_2\left(\rho_2 c_2^2 - \beta_2\right)}{\rho_2 C_2^2} + \frac{\alpha_1\left(\rho_1 c_1^2 - \beta_1\right)}{\rho_1 C_1^2}\right)\frac{\partial u}{\partial x} \right. \\ & \quad - \left(\frac{\rho_2 c_2^2 - \beta_2}{\rho_2^2 C_2^2} - \frac{\rho_1 c_1^2 - \beta_1}{\rho_1^2 C_1^2}\right)\frac{\partial(\rho\, Y_1 Y_2 u_R)}{\partial x} \\ & \quad \left. -\rho\, Y_1 Y_2 u_R \left(\frac{\Gamma_2 T_2}{\rho_2 C_2^2}\,\frac{\partial s_2}{\partial x} - \frac{\Gamma_1 T_1}{\rho_1 C_1^2}\,\frac{\partial s_1}{\partial x}\right)\right] = \Gamma\,\lambda\, u_R^2. \end{aligned} \quad (C\,28)$$

https://doi.org/10.1017/S0022112010003794 Published online by Cambridge University Press

During the diffusion step, part only of the volume fraction equation (C 3) has been considered. Consequently, constraints become out of equilibrium at the end of the diffusion step.

C.2.4. *Pressure relaxation and reset steps*

Now it remains to solve the following system, under the constraint $\pi_1 = \pi_2$:

$$\left.\begin{aligned}
&\frac{\partial \alpha_1}{\partial t} = -\rho C_W^2 \frac{\alpha_1 \alpha_2}{\rho_1 C_1^2 \rho_2 C_2^2} \rho Y_1 Y_2 u_R \left(\frac{\Gamma_1}{\alpha_1} T_1 \frac{\partial s_1}{\partial x} + \frac{\Gamma_2}{\alpha_2} T_2 \frac{\partial s_2}{\partial x} \right), \\
&(\alpha\rho)_1 \frac{\partial e_1}{\partial t} = -P_1 \frac{\partial \alpha_1}{\partial t}, \\
&(\alpha\rho)_2 \frac{\partial e_2}{\partial t} = +P_2 \frac{\partial \alpha_1}{\partial t}, \\
&\frac{\partial (\alpha\rho)_1}{\partial t} = 0, \\
&\frac{\partial (\alpha\rho)_2}{\partial t} = 0, \\
&\frac{\partial (\rho u)}{\partial t} = 0, \\
&\frac{\partial (\rho E)}{\partial t} = 0.
\end{aligned}\right\} \qquad \text{(C 29)}$$

Resolution of that system is done in a way similar to what has been done during the hyperbolic pressure relaxation step.

REFERENCES

Abgrall, R. 1996 How to prevent pressure oscillations in multicomponent flow calculations: a quasi-conservative approach. *J. Comput. Phys.* **125**, 150–160.

Alderborn, G. & Nyström, C. (Ed.) 1996 *Pharmaceutical Powder Compaction Technology*. Marcel Dekker.

Baer, M. & Nunziato, J. 1986 A two-phase mixture theory for the deflagration-to-detonation transition ddt in reactive granular materials. *Intl J. Multiphase Flows* **12**, 861–889.

Bdzil, J., Menikoff, R., Son, S., Kapila, A. & Stewart, D. 1999 Two-phase modelling of ddt in granular materials: a critical examination of modelling issues. *Phys. Fluids* **11**, 378–402.

Chinnayya, A., Daniel, E. & Saurel, R. 2004 Computation of detonation waves in heterogeneous energetic materials. *J. Comput. Phys.* **196**, 490–538.

Duberg, M. & Nyström, C. 1986 Studies on direct compression of tablets XVII. Porosity-pressure curves for the characterization of volume reduction mechanisms in powder compression. *Powder Technol.* **46**, 67–75.

Elban, W. & Chiarito, M. 1986 Quasi-static compaction study of coarse HMX explosive. *Powder Technol.* **46** (2–3), 181–193.

Favrie, N., Gavrilyuk, S. & Saurel, R. 2009 Diffuse solid-fluid interface model in cases of extreme deformations. *J. Comput. Phys.* **228**, 6037–6077.

Gethin, D., Tran, V., Lewis, R. & Ariffin, A. 1994 An investigation of powder compaction processes. *Intl J. Powder Metall.* **30** (4), 385–398.

Gonthier, K. 2003 Modelling and analysis of reactive compaction for granular energetic solids. *Combust. Sci. Technol.* **175** (9), 1679–1709.

Gonthier, K. 2004 Predictions for weak mechanical ignition of strain hardened granular explosive. *J. Appl. Phys.* **95** (7), 3482–3494.

Guillard, H. & Duval, F. 2007 A Darcy law for the drift velocity in a two-phase flow model. *J. Comput. Phys.* **224**, 288–313.

https://doi.org/10.1017/S0022112010003794 Published online by Cambridge University Press

Jogi, V. 2003 Predictions for multi-scale shock heating of a granular energetic material. Master's Thesis, Louisiana State University. Available at: http://etd.lsu.edu/docs/available/etd-0811103-164117/.

Kapila, A., Menikoff, R., Bdzil, J., Son, S. & Stewart, D. 2001 Two-phase modelling of ddt in granular materials: reduced equations. *Phys. Fluids* **13** (10), 3002–3024.

Karni, S. 1994 Multicomponent flow calculations by a consistent primitive algorithm. *J. Comput. Phys.* **112**, 31–43.

Khasainov, B., Borisov, A., Ermolaev, B. & Korotkov, A. 1981 Two-phase visco-plastic model of shock initiation of detonation in high density pressed explosives. In *Seventh International Symposium on Detonation* (ed. Office of Naval Research), pp. 435–447. Naval Surface Weapons Center, Annapolis, MD.

Kuo, K., Yang, V. & Moore, B. 1980 Intragranular stress, particle-wall friction and speed of sound in granular propellant beds. *J. Comput. Phys.* **4** (1), 697–730.

Le Métayer, O., Massoni, J. & Saurel, R. 2004 Élaboration des lois d'état d'un liquide et de sa vapeur pour les modèles d'écoulements diphasiques (in French). *Intl J. Therm. Sci.* **43**, 265–276.

Lewis, R. & Khoei, A. 2001 A plasticity model for metal powder forming processes. *Intl J. Plast.* **17**, 1659–1692.

Martin, C., Bouvard, D. & Shima, S. 2003 Study of particle rearrangement during powder compaction by the discrete element method. *J. Mech. Phys. Solids* **51** (4), 667–693.

Murrone, A. & Guillard, H. 2005 A five equations reduced model for compressible two-phase flow problems. *J. Comput. Phys.* **202**, 664–698.

Oliver, J., Oller, S. & Cante, J. 1996 A plasticity model for simulation of industrial powder compaction processes. *Intl J. Solids Struct.* **33** (20), 3161–3178.

Passman, S., Nunziato, J. & Walsh, E. 1984 A theory of multiphase mixtures. In *Rational Thermodynamics* (ed. C. Trusdell), Appendix 5c, pp. 286–325. Springer.

Périgaud, G. & Saurel, R. 2005 A compressible flow model with capillary effects. *J. Comput. Phys.* **209**, 139–178.

Petitpas, F., Massoni, J., Saurel, R., Lapebie, E. & Munier, L. 2009 Diffuse interface models for high speed cavitating underwater systems. *Intl J. Multiphase Flow* **35**, 747–759.

Rogue, X. 1997 Expériences et simulations d'écoulements diphasiques en tubes à choc (in French). PhD Thesis, Université de Provence, Marseille, France.

Rogue, X., Rodriguez, G., Haas, J. & Saurel, R. 1998 Experimental and numerical investigation of the shock-induced fluidization of a particle bed. *Shock Waves* **8**, 29–45.

Sandusky, H. & Liddiard, T. 1985 Dynamic compaction of porous bed of porous beds. *Tech. Rep.* NSWC TR 83-246. Naval Surface Weapons Center.

Saurel, R. & Abgrall, R. 1999 A multiphase Godunov method for compressible multifluid and multiphase flows. *J. Comput. Phys.* **150**, 425–467.

Saurel, R., Gavrilyuk, S. & Renaud, F. 2003 A multiphase model with internal degree of freedom: application to shock-bubble interaction. *J. Fluid Mech.* **495**, 283–321.

Saurel, R., Petitpas, F. & Abgrall, R. 2008 Modeling phase transition in metastable liquids. Application to flashing and cavitating flows. *J. Fluid Mech.* **607**, 313–350.

Saurel, R., Petitpas, F. & Berry, R. 2009 Simple and efficient relaxation methods for interfaces separating compressible fluids, cavitating flows and shocks in multiphase mixtures. *J. Comput. Phys.* **228**, 1678–1712.

Wood, A. 1930 *A Textbook of Sound*. G. Bell and Sons Ltd.

https://doi.org/10.1017/S0022112010003794 Published online by Cambridge University Press